1-5-2022

Deep Extragalactic VIsible Legacy Survey: Data Release 1 blended spectra search for candidate strong gravitational lenses

Benne Holwerda
University of Louisville, benne.holwerda@louisville.edu

S Knabel

J E. Thorne

S Bellstedt

M Siudek

See next page for additional authors

Original Publication Information

ThinkIR Citation

Authors

Benne Holwerda, S Knabel, J E. Thorne, S Bellstedt, M Siudek, and L J M Davies

Deep Extragalactic VIsible Legacy Survey: Data Release 1 blended spectra search for candidate strong gravitational lenses

B. W. Holwerda [iD],[1]★ S. Knabel,[1] J. E. Thorne,[2] S. Bellstedt [iD],[2] M. Siudek [iD][3,4] and L. J. M. Davies [iD][2]

[1]*Department of Physics and Astronomy, University of Louisville, 102 Natural Science Building, Louisville, KY 40292, USA*
[2]*ICRAR, The University of Western Australia, 35 Stirling Highway, Crawley, WA 6009, Australia*
[3]*Institut de Física d'Altes Energies (IFAE), The Barcelona Institute of Science and Technology, E-08193 Bellaterra (Barcelona), Spain*
[4]*National Centre for Nuclear Research, ul. Pasteura 7, PL-02-093 Warsaw, Poland*

ABSTRACT

Here, we present a catalogue of blended spectra in Data Release 1 of the Deep Extragalactic VIsible Legacy Survey (DEVILS) on the Anglo-Australian Telescope. Of the 23 197 spectra, 181 showed signs of a blend of redshifts and spectral templates. We examine these blends in detail for signs of either a candidate strong lensing galaxy or a useful overlapping galaxy pair. One of the three DEVILS target fields, COSMOS (D10), is close to complete and it is fully imaged with *Hubble Space Telescope* Advanced Camera for Surveys, and we visually examine the 57 blended spectra in this field in the *F814W* postage stamps. Nine are classical strong lensing candidates with an elliptical as the lens, out to higher redshifts than any previous search with spectroscopic surveys such as Sloan Digital Sky Survey (SDSS) or Galaxy And Mass Assembly. The gravitational lens candidate success rate is similar to earlier such searches (0.1 per cent). Strong gravitational lenses identified with blended spectroscopy have typically shown a high success rate (>70 per cent), which make these interesting targets for future higher resolution lensing studies, monitoring for supernova cosmography, or searches for magnified atomic hydrogen signal.

Key words: gravitational lensing: strong – catalogues – surveys – galaxies: distances and redshifts.

1 INTRODUCTION

Strong gravitational lenses occur when a massive, distant galaxy – the lens – aligns with an even more distant galaxy – the source – and bends the light from the source into our line of sight. Strong gravitational lensing provides a highly accurate measurement of the *total* enclosed mass in these elliptical galaxies, which is robust when compared against current galaxy evolution models and assumptions (Shu et al. 2015, and reference therein). Gravitational lensing provides the best estimate of the total projected mass of the lens galaxy enclosed within the Einstein radius, delineated by the arcs projected on the sky from the background source galaxy.

As such, lensing elliptical galaxies may provide an excellent test case for other theories of gravity, such as the emergent gravity recently proposed by Verlinde (2017), through a combination of lensing and kinematic measurements (see Tortora et al. 2018). To date, gravitational lenses have proven general relativity to be correct with the highest accuracy over galaxy-wide scales (Collett et al. 2018).

Because strong gravitational lenses appear in every respect to be just like other (elliptical) galaxies, results can therefore be generalized to all spheroidal galaxies *in the observed mass range* (Auger et al. 2009). Gravitational lensing has been a powerful technique to measure the masses of *massive* elliptical galaxies (Gavazzi et al. 2007; Bolton et al. 2008a), constraining the Fundamental Plane (r_e–

M_*–σ) of elliptical galaxies (Bolton et al. 2008b), and the stellar population's mass-to-light ratio (M/L) and thus their initial mass function (IMF; Auger et al. 2009).

The observational drive for classical galaxy–galaxy strong lenses – an elliptical galaxy as a lens with an emission-line galaxy (ELG) as the source – is now to measure the mass content throughout the spheroidal galaxy mass function (Shu et al. 2015), explore the Fundamental Plane in different environments (Treu et al. 2009), constrain the stellar M/L in nearby ellipticals (Treu et al. 2006; Collier, Smith & Lucey 2018a,b), and to discover dark matter substructure in known strong galaxy lens cases (Cyr-Racine, Keeton & Moustakas 2019). Thanks to integral field unit (IFU) surveys, lensing arcs no longer need to be well outside the lens galaxy's isophote (Lee 2017; Smith 2017; Talbot et al. 2018; Smith et al. 2020).

Thus far, lensing arcs have predominantly been identified in *massive* ($>10^{11}$ M$_\odot$) spheroidal lens systems, thanks to selection biases: SDSS spectroscopic targets are volume-weighted to greater mass, and visual identification favours well-separated arc and lens (Shu et al. 2015). The spectroscopically selected sample from the Galaxy And Mass Assembly (GAMA) spectroscopic survey (Driver et al. 2009; Liske et al. 2015) opened a much greater range in lens masses, thanks to the higher completeness and depth of GAMA (Holwerda et al. 2015). Spectroscopic identification of lensing galaxies has had a high rate of confirmation, e.g. Chan et al. (2016) reported a >70 per cent confirmation rate for a subset of 14 of the Holwerda et al. (2015) and Knabel et al. (2020) lens candidates. Similar numbers have been reported for the Strong Lenses with ACS (SLACS) survey.

★ E-mail: benne.holwerda@gmail.com

Since the first spectroscopy successes, the search for classical strong gravitational lenses has entered a rapid expansion with the use of machine learning or citizen science on deeper and high-resolution ground-based surveys (Petrillo et al. 2017, 2019a,b; Jacobs et al. 2019; Huang et al. 2020; Li et al. 2020). The trade-off is between high levels of confidence in individual sources (spectroscopy) or larger target samples that still need confirmation and redshifts (machine learning). The three identification methods are very much complementary in redshift and mass as a comparison between the GAMA spectroscopic and KiDS machine learning and citizen science identifications in the three GAMA equatorial fields as shown in Knabel et al. (2020). One can confirm machine learning identified strong lenses in a spectroscopic survey using the cross-correlation metrics discussed below (Knabel et al., in preparation).

Candidate strong lenses, even presently unresolved, are valuable potential targets for follow-up monitoring for lensed supernova light curves (Oguri 2010; Shu et al. 2018; Goldstein, Nugent & Goobar 2019; Wojtak, Hjorth & Gall 2019; Holwerda et al. 2021) for use of supernova time-delay cosmography, the independent measure of the Hubble constant (H_0) from the delay between lensed images (see the reviews by Treu & Marshall 2016; Oguri 2019). As long as redshifts for lens and source galaxy are accurately known, the time delay primarily depends on the Hubble constant.

The search, confirmation, and scientific use of strong gravitational lensing systems is expected to change once more with the advent of sensitive and high spatial resolution surveys for atomic hydrogen (H I). Lipnicky et al. (2018) report the first strongly lensed H I detection using a nearby edge-on spiral galaxy as the lens. The new H I surveys, such as MIGHTEE (Jarvis et al. 2016; Delhaize et al. 2021; Maddox et al. 2021) and LADUMA (Holwerda 2011; Blyth 2015; Blyth et al. 2016; Baker et al. 2018) using the MeerKAT radio telescope and WALLABY (Koribalski et al. 2020) on ASKAP (Johnston et al. 2008), promise a boon of H I detections lensed by a closer galaxy (Deane, Obreschkow & Heywood 2015; Blecher et al. 2019). A magnified H I detection would allow these surveys to probe below their sensitivity limit to verify, for example, the results from stacking H I spectra for a given galaxy population (cf. Delhaize et al. 2013; Chowdhury et al. 2020, 2021; Healy et al. 2021).

Deane et al. (2015) made a prediction that the CHILES and LADUMA deep H I fields (COSMOS and CDF-S, respectively) host a single strong lens to dozens respectively. Depending on spectroscopic coverage and volume, more strong H I lenses can be found in MIGHTEE and WALLABY. Blended optical spectra would point to where to look in position and frequency in the H I cubes. The benefit of H I confirmation is that it need not rely on a classical galaxy–galaxy gravitational lens, i.e. an elliptical or spheroidal galaxy acting as the lens. Any galaxy along the line of sight would be sufficient to magnify the source H I signal. With this in mind, we report the positions and redshifts of all the blended spectra in this paper.

The successor of GAMA and the precursor of the WAVES survey[1] is underway on the Anglo-Australian Telescope (AAT): the Deep Extragalactic VIsible Legacy Survey (DEVILS; Davies et al. 2018). The DEVILS survey goes to a greater depth and higher redshift range than GAMA with the same high level of completeness. We present the candidate search as a pathfinder for the near-future strong lenses searches using spectroscopy. Here, we report the candidate strong gravitational lenses identified in the three fields targeted in the DEVILS survey specifically to facilitate follow-up observations,

e.g. searches for magnified H I signal or doubly imaged supernovae with a time delay.

This paper is organized as follows: Section 2 describes the DEVILS data products used, Section 3 describes the selection of blended spectra, Section 4 presents the characteristics for the three DEVILS target fields, Section 5 discusses the COSMOS (D10) field Hubble imaging of blended spectra, and Section 6 comprises our concluding remarks for this catalogue result. Throughout this paper, we adopt a Planck Collaboration (2014) cosmology ($H_0 = 67.7$ km s^{-1} Mpc^{-1} and $\Omega_\mathrm{m} = 0.307$).

2 DEVILS

DEVILS (Davies et al. 2018) is a large spectroscopic campaign at the AAT (Sharp et al. 2006) aimed at bridging the near and distant Universe by producing a high completeness survey of galaxies and groups at intermediate redshifts ($0.3 < z < 1.0$). The target sample consists of $\sim 60\,000$ galaxies selected down to $Y < 21.2$ mag, over ~ 6 deg^2 spread over three well-studied deep extragalactic fields: the Cosmic Origins Survey (COSMOS) field (DEVILS D10 field), the Extended Chandra Deep Field-South (ECDF-S, D03), and the X-ray Multi-Mirror Mission Large-Scale Structure (XMM-LSS) region (D02).

These three fields are all 'deep drilling fields' for the Legacy Survey of Space and Time on the Vera C. Rubin Telescope. Target selection for DEVILS is from Y-band imaging performed by the deep Visible and Infrared Survey Telescope for Astronomy (VISTA) extragalactic observations: VIDEO (Jarvis et al. 2013) and UltraV-ISTA (McCracken et al. 2012), with photometry measured using the PROFOUND package (Robotham et al. 2018). Photometric star/galaxy separation is done on the basis of near-infrared colours and has been validated by visual inspection described in Davies et al. (in preparation). These fields are the prime targets for the MIGHTEE (Jarvis et al. 2016; Delhaize et al. 2021; Maddox et al. 2021), LADUMA (Holwerda 2011; Blyth 2015; Blyth et al. 2016; Baker et al. 2018), and CHILES (Dodson et al. 2016; Fernández et al. 2016; Jones et al. 2016; Hess et al. 2019; Blue Bird et al. 2020) deep H I surveys.

We will focus on the COSMOS (Scoville et al. 2007) field (DEVILS D10) in Section 5 because it is the closest to full completion of the three DEVILS fields and it has complete complementary *Hubble Space Telescope* (*HST*) archival imaging data. Blended spectra candidates from the other two fields, XMM-LSS (D02) and ECDF-S (D03), are presented for future follow-up. The field represents an early opportunity where lensed H I could be found in the CHILES survey (Fernández et al. 2016).

3 STRONG LENS SELECTION

Strong lensing candidates are selected from a clear double signal in the spectrum's redshift cross-correlation fits with spectral templates. We note that the searches for a double signal in an observed spectrum can have two scientific motivations. One can look for lensing systems such as the original SLACS project (Bolton et al. 2006). SDSS blended spectra, i.e. passive galaxy (PG) spectra with one or more emission lines obviously at a higher redshift, were highly successful identifying strong gravitational lenses (70 per cent efficacy) for follow-up and analysis with Hubble. A similar success rate was reported by Chan et al. (2016) for the Holwerda et al. (2015) selections. Alternatively, one searches for overlapping galaxies that can be used to estimate galaxy transparency based on differential photometry (Domingue et al. 1999a,b; Domingue, Keel & White 2000; White, Keel & Conselice 2000; Keel & White 2001a,b; Holwerda, Keel &

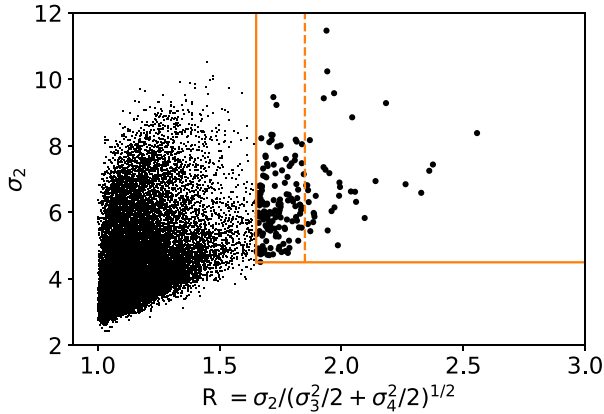[1]Wide Area Vista Extragalactic Survey (Driver et al. 2019).

Figure 1. The value of R and the height of the second cross-correlation peak (σ_2). The selection of strong candidates for blended spectra is shown as the solid orange line. The original R criterion from Holwerda et al. (2015) is shown as the dashed line. In the selected cases, there is a high second peak that is much higher relative to the subsequent ones.

Bolton 2007; Holwerda et al. 2009, 2013; Holwerda & Keel 2013, 2017). The latter was the original motivation for the search in SDSS (Holwerda et al. 2007) and GAMA (Holwerda et al. 2015) for blended spectra.

3.1 AUTOZ

The redshifts in the DEVILS survey are found using the cross-correlation software AUTOZ (Baldry et al. 2014). This uses a series of templates and cross-correlates them with the spectra, producing a ranking of redshift and template combinations with different strengths of correlation. This often leads to a second cross-correlation peak because of a strong emission line being misidentified at the incorrect redshift (aliasing). These are not likely candidates for a gravitational lens but cannot entirely be discounted because a strong lens might just lie on such a caustic.

The DEVILS Data Release 1 (DR1) AUTOZ catalogue has 23 197 entries based on AAT spectroscopy and any archival spectra of similar or better quality. This first science release DR1 of DEVILS is about a third towards its science goal of 60 000 redshifts complete with ancillary products in three science fields.

3.2 Blended spectra

Strong lenses can be identified from a second cross-correlation peak that is much stronger than the third or fourth one and consists of the first, highest cross-correlation peak at a lower redshift with a passive template (no or few emission lines) and a second cross-correlation peak at a higher redshift with a strong emission-line spectrum template. We follow the same setup as in Holwerda et al. (2015) for the AUTOZ catalogue from the DEVILS fields. We define the R value as follows:

$$R = \frac{\sigma_2}{\sqrt{\sigma_3^2/2 + \sigma_4^2/2}}, \quad (1)$$

where σ_n is the height of the cross-correlation peak for the nth ranked redshift and template combination.

Fig. 1 shows the values for R and σ_2 (the height of the second cross-correlation peak) in the DEVILS spectroscopic AUTOZ catalogue. We opt for a slightly wider set of criteria (in R and σ_2) than Holwerda et al. (2015) with a lower threshold for the R values. A comparison
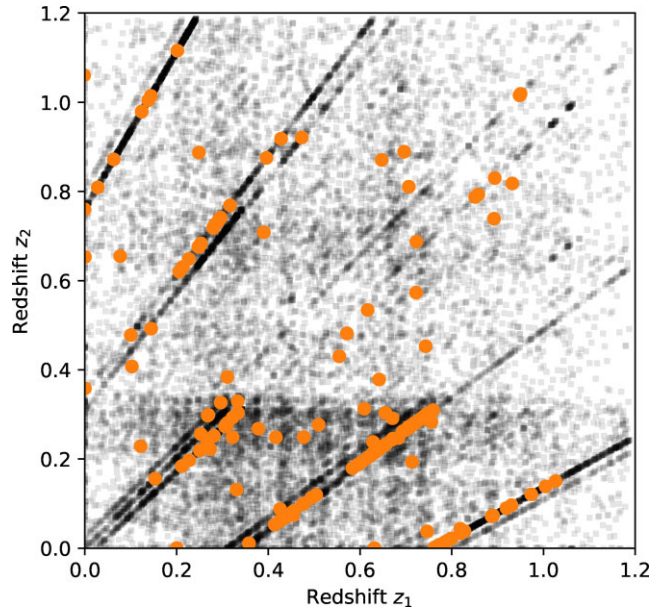

Figure 2. The first and second redshifts as identified by AUTOZ. Alias lines are visible as diagonal lines of points. A number of the candidates selected in Fig. 1 are on such alias lines.
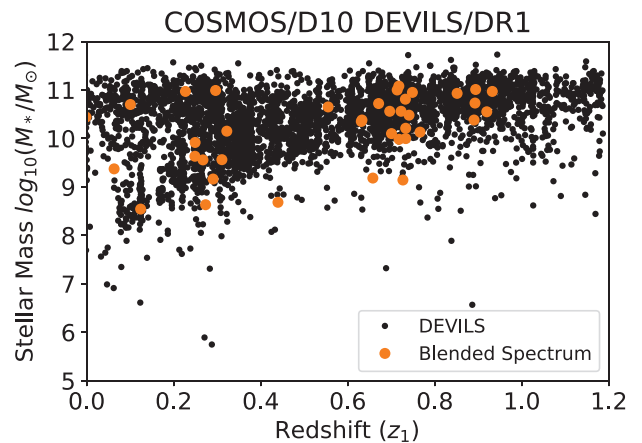

Figure 3. The redshift versus stellar mass plot for the DEVILS DR1 in COSMOS/D10 with blended spectra marked with orange markers. DEVILS DR1 is complete to $\log(M^*) \sim 9.5$ out to $z \sim 1$. Blended spectra appear to be mostly within the completeness envelope.

between AUTOZ of machine learning identified strong lenses (Knabel et al., in preparation) has shown that the original criterion was very conservative in R. Spectra with a relatively high second cross-correlation peak are our blended spectra targeted for further scrutiny.

Fig. 2 shows the first and second peak redshifts for all the DEVILS spectra and those selected as blended spectra systems. A large number of these are on aliasing lines and may well be artefacts of the AUTOZ fits. However, this does not preclude them from being a strong gravitational lens candidate. For example, candidates on aliasing lines were later confirmed as strong lenses (Knabel et al. 2020). For a search of magnified H I, we argue that a wide net of candidate positions and redshifts is most practical.

Fig. 3 shows the redshift of the primary cross-correlation and the stellar mass for COSMOS/D10 from Thorne et al. (2021), derived from the PROFOUND photometry (Davies et al., in preparation) using
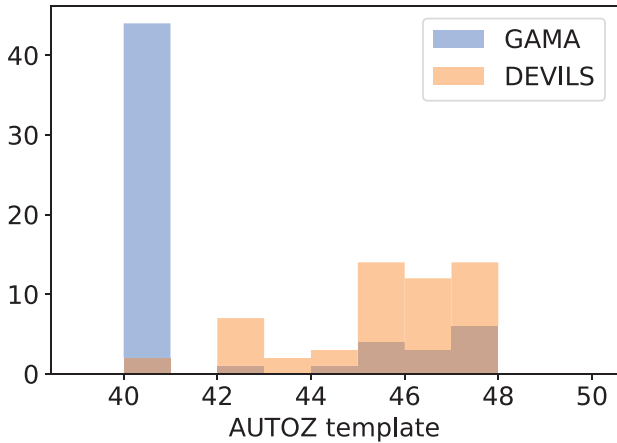
Figure 4. The histogram of template numbers (lower meaning more passive templates) for the GAMA blended spectra from Holwerda et al. (2015) and those from the DEVILS DR1 catalogue.

the PROSPECT tool (Robotham et al. 2020). DEVILS DR1 is complete to $\log(M_*/M_\odot) \sim 9.5$ out to $z \sim 1$. Blended spectra are mostly within this completeness envelope and follow redshift overdensities due to large-scale structure because these increase the odds of two galaxies along the line of sight.

3.3 Templates

Fig. 4 shows the template distribution from the AUTOZ for the lowest redshift galaxy for the new DEVILS blended spectra and those from Holwerda et al. (2015). To broadly classify the templates, Holwerda et al. (2015) classify templates 40–42 as 'PGs' and 43–47 as 'ELGs'. The GAMA lens candidates were selected to prefer passive templates, while the DEVILS candidate selection is a mix of passive and emission-line templates. There is a different mix of templates in DEVILS because it probes to an earlier epoch and therefore contains more ELGs. Our lower selection threshold may contain more contamination from aliasing strong emission lines. DEVILS is still being completed and a signal-to-noise ratio (S/N) is still being accumulated for a successful redshift with stellar continuum dominated sources (PG) and a higher completeness in the target regions.

Fig. 5 shows a few example DEVILS spectra for the COSMOS fields. Expected emission and absorption features are marked for both of the cross-correlation solutions (z_1 and z_2). It illustrates how certain spectral features drive a high cross-correlation with the AUTOZ templates.

4 RESULTS

4.1 DEVILS fields

Fig. 6 shows the positions of DEVILS DR1 redshifts spread over the three fields. Of these three, COSMOS (D10) is the most complete. We identify 57 blended spectra in COSMOS, 75 in XMM-LSS, and 49 in ECDF-S, which would be too high for the expected on-sky number density of strong lenses alone (see the discussion in Knabel et al. 2020), but an equal number of galaxy–galaxy alignments is expected (e.g. the overlapping pairs of galaxies; Holwerda et al. 2015).

Table 1 lists the number of spectra and the number of blended spectra identified in DEVILS DR1. Table 2 lists all the candidate

strong lenses in D10 (COSMOS) in DEVILS DR1. Typically, 0.1 per cent of a large survey is a blended source (Holwerda et al. 2015), but the rate is closer to 1 per cent in DEVILS. This is partly due to the lower threshold in R we set as well as the high completeness to a lower apparent magnitude of the survey, increasing the chances of alignments along the line of sight. We expect however that the majority of the blended spectra are chance alignments and not strong gravitational lenses.

Fig. 7 shows the stellar mass from the PROSPECT (Robotham et al. 2020) spectral energy density fit to the DEVILS photometry and the first peak redshift in the COSMOS (DEVILS/D10) field. We compare these to masses and redshifts from Holwerda et al. (2015) and the SLACS (Bolton et al. 2008a) and SLACS for the Masses (S4TM; Shu et al. 2017) values. We note here that the values from Holwerda et al. (2015) are also derived using MAGPHYS. The SLACS values are reported for both a Salpeter and a Charbrier IMF and are used to infer an M/L for the Johnson I *HST* observation. The wider aperture for SDSS spectra (3 arcsec) allows for the selection of more massive systems at a lower redshift (see Knabel et al. 2020).

Fig. 7 shows how the SLACS and S4TM probe massive systems ($\log(M_*/M_\odot) > 11$) below $z \sim 0.5$. The high completeness and depth of GAMA (together with narrower fibre aperture) resulted in a lens sample that is both at higher redshifts for the same mass and lower masses at low redshifts. The expectation for DEVILS is that the final lens candidate sample from this survey probes both higher redshifts again and lower masses at intermediate redshifts. The DEVILS markers in Fig. 7 are all the blended spectra without additional constraints. However, these include indeed lower masses at low redshifts ($z < 0.3$) and higher redshift candidates at the high-mass end ($0.5 < z < 1$).

4.2 Predicted Einstein radii

To estimate the Einstein radius of the candidate lenses, we approximate the galaxy lens as a thin-lens system with the lens and source positioned along the same line of sight, where the Einstein radius (θ_E) is given by

$$\theta_E = \sqrt{\frac{M_E}{10^{8.09}\,M_\odot}} \sqrt{\frac{D_{LS}}{D_L D_S}\,\text{Mpc}}\ \text{arcsec}, \tag{2}$$

where M_E is the total *enclosed* mass by the Einstein radius, D_{LS} is the distance from a lens to a source, D_L is the distance from an observer to a lens, and D_S is the distance from an observer to a source. All distances are angular diameter distances calculated from redshift assuming flat Λ cold dark matter.

Auger et al. (2010) modelled and analysed 73 SLACS lenses and presented a power-law relation between the total (lensing) mass enclosed within half the effective radius (close to the typical Einstein radius) and the stellar mass:

$$M_E = 0.0011 \times \left(\frac{M_*}{M_\odot}\right)^{1.25}. \tag{3}$$

Fig. 8 shows a histogram of predicted Einstein radii for the GAMA blended spectra from Holwerda et al. (2015) and those from DEVILS DR1. A majority of DEVILS blended spectra predict Einstein radii of 0.1 arcsec or below. In practice, we have found that the above estimate underpredicts the Einstein radii fractionally (Knabel et al., in preparation). Nevertheless, such compact lenses are incredibly difficult to meaningfully resolve, even with the *HST* or a ground-based Adaptive Optics (AO) system with an IFU, but they may prove
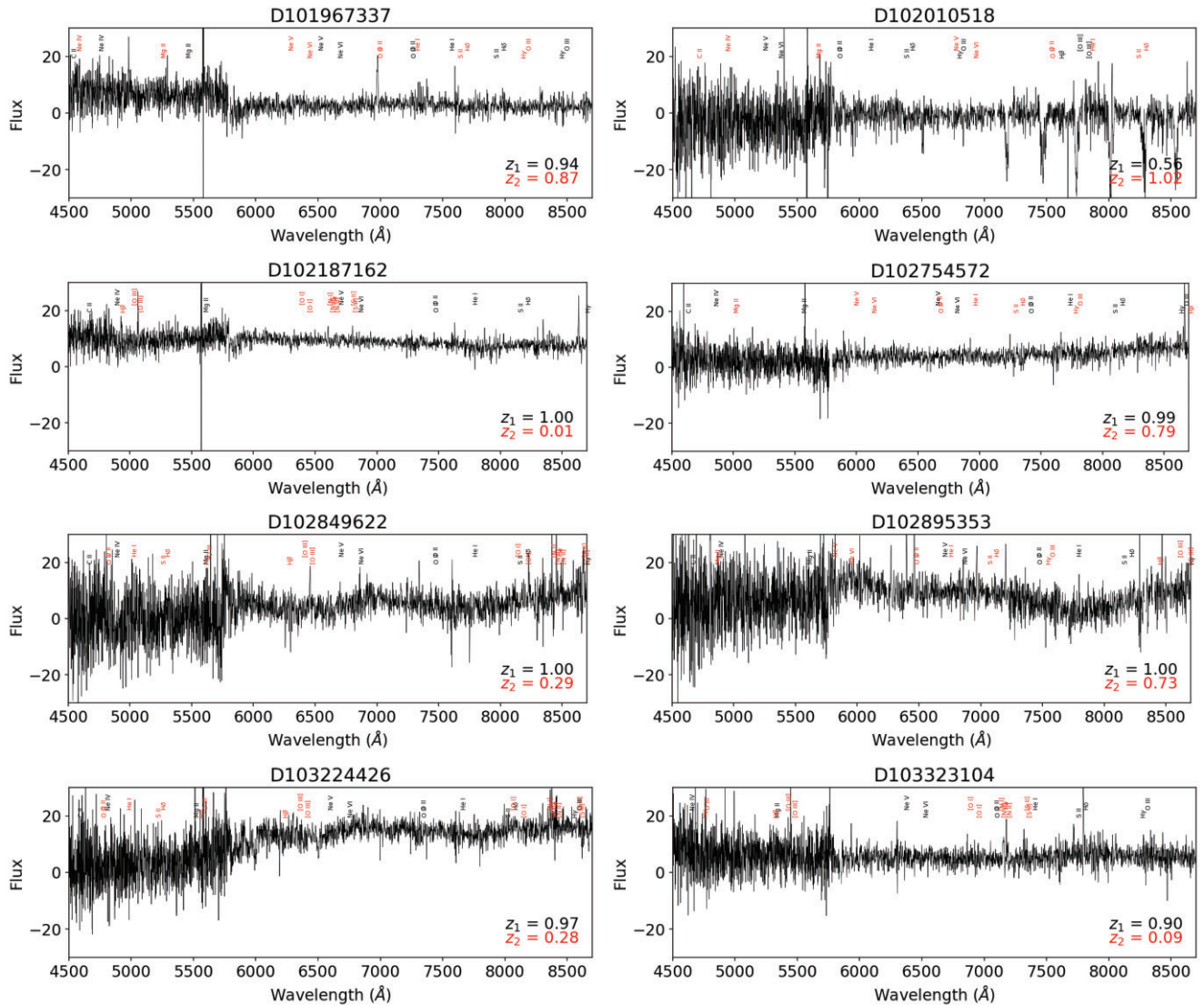
Figure 5. Native DEVILS spectra in the COSMOS region with two redshift solutions that make our cross-correlation cut. Emission and absorption lines are marked for the first (black) and second (red) redshift solutions. An alternate view is shown in Fig. A1.
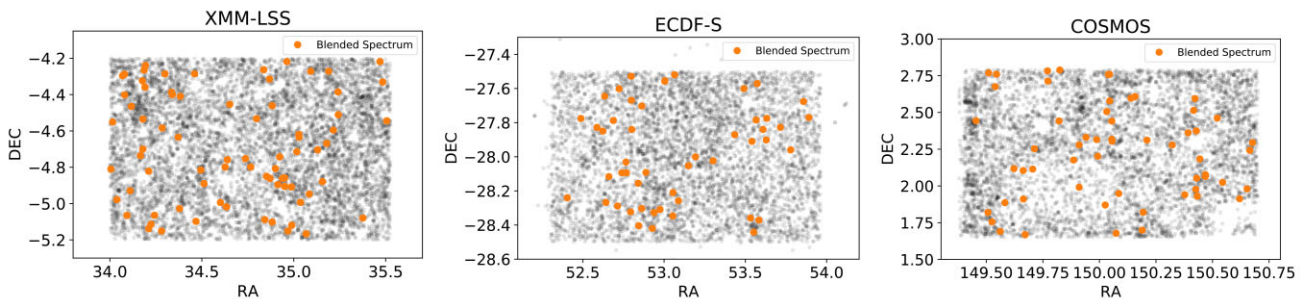

Figure 6. The positions of the DEVILS spectra in all three fields.

worthwhile targets for searches for magnified H I lines or a next generation of AO-enabled telescopes.

The odds that no magnified stellar emission can be observed go up with a smaller Einstein ring. The magnification of the lens goes as $\mu = \frac{|\theta|}{|\theta| - \theta_E}$, where $|\theta|$ is the angular distance between a source and a lens in the image plane and θ_E is the Einstein radius (cf.

Mason et al. 2015). With small Einstein radii, the sources have to overlap in the image plane to produce high magnifications, i.e. there has to be a meaningful cross-section between the extent of the star formation nebular line and stellar emission of the background galaxy and the caustic for there to be a detectable signal and ring, respectively.

Table 1. DEVILS DR1 fields and the number of blended spectra identified in each.

DEVILS name	Common name	RA (°)	Dec. (°)	Input survey	No. of spectra	Blended spectra
D02	XMM-LSS	35.4975	−4.825	VIDEO	9402	75
D03	ECDF-S	53.65	−28.1	VIDEO	6574	49
D10	COSMOS	150.1	2.1	UltraVISTA	7219	57

The selection of sources as lenses depends on the survey considered and what level of magnification is considered a lens. Dobler et al. (2008) modelled Sloan (SDSS) spectra to estimate the selection function of the SLACS survey. They had to account for the size of the source galaxies in emission-line regions (e.g. O II emitting parts of star-forming galaxies at a higher redshift). Most recent authors examined the selection functions of photometric imaging surveys for strong lenses (Chang et al. 2015; Collett 2015, 2017). Dobler et al. (2008) estimated high probabilities for false positives (80 per cent and above), with higher false-positive rates for high ($z \sim 0.4$) redshift lenses. Extrapolating the trends seen in Dobler et al. (2008) can lead to higher false-positive rates for DEVILS (higher redshift lens galaxies) or lower magnifications. For a pair of galaxies along the line of sight to be selected, they need not be lensing [defined as a magnification of at least $\mu = 1.5$ by Dobler et al. (2008)]. Compared to their fig. 5, the GAMA lens rate of 70 per cent confirmed (Chan et al. 2016) of 0.05 per cent of the survey is typical for $\mu = 2$ magnifications.

The verification of these lenses through magnified H I emission is a different proposition however. H I discs are much more extended than the star-forming counterpart (cf. de Blok et al. 2020; Wang et al. 2021) and closer to uniform in surface brightness. While the Einstein radius may not shrink, the angular separation of source and lens will. The rate of unassociated emission lines becomes commensurately lower and the lensing effect greater. With a position and redshift to look for these lenses in an H I cube, together with likely a magnification factor of several to ten times, makes these DEVILS targets more likely to be galaxy-galaxy H I lenses.

5 *HST* IMAGING

For one of the fields, COSMOS (D10), there is uniform *HST*/Advanced Camera for Surveys (ACS) imaging from the COSMOS collaboration (Scoville et al. 2007), and it is straightforward to obtain image cutouts.[2] Fig. 9 shows all the 56 blended spectra for which a cutout is available. These cutouts are not available for the other two DEVILS fields. The majority appear to be chance alignments in the aperture of the AAT spectrograph, i.e. a genuine occulting galaxy pair.

Despite the high resolution of these images, they are not ideal to visually identify strong lenses. The COSMOS field was observed in the *F814W* filter (broad Johnson *I*), and this is good to map the stellar mass of higher redshift galaxies; a blue filter (*F606W* of *F555W*, i.e. Johnson *V*) is typically used to identify the source galaxy in a strong gravitational lens.

Given the limited information in a single-filter, shallow *HST* image, we limit our visual classification to spiral–elliptical, spiral–spiral, or elliptical–elliptical superpositions or 'lens candidate' (elliptical with possible circular structure), the same as in Holwerda et al. (2015). This is a visual estimate of which galaxy looks in front

as well the broad morphological type. In Holwerda et al. (2015), we found that the visual classification (based on SDSS imaging) and the template matches were relatively poor, and deeper and higher resolution imaging confirmed strong lens candidates (Chan et al. 2016). We note which systems may be useful for a future study of dust transparency using the occulting galaxy method (cf. Holwerda & Keel 2016, 2017), a partial overlap of two galaxies with good apparent symmetry.

The total of blended spectra that are marked as potential classical lenses (the lensing galaxy is a foreground elliptical) after visual inspection is nine (~ 0.1 per cent of DEVILS DR1 on D10, Fig. 10), which is more in line with expectations from previous searches for lenses and overlapping galaxies in spectroscopic surveys (Holwerda et al. 2007, 2015). One should consider these confirmed actual lenses if multicolour *HST* imaging, high-resolution AO-enabled IFU, or magnified H I can verify their nature.

6 CONCLUDING REMARKS

In this paper, we report the blended spectra in DEVILS DR1. For the COSMOS (D10) field, nine classical candidate lenses (elliptical galaxies as the potential lens) are identified with DEVILS promising to deliver more distant strong gravitational lenses than any previous survey. We stress that these are candidates to be confirmed still with other methods (AO imaging, an IFU map, or lensed H I at the source galaxy). At the distance out to which DEVILS can identify strong lenses, resolving the characteristic arc may become challenging for even the most high resolution imaging. IFU and AO may help disentangle the signal from lens and source, and the detection of H I line at the source redshift is considered strong confirmation. We note that for H I lensing events, the lensing galaxy need not be an elliptical. Change alignment would allow the H I signal to be magnified by any galaxy mass along the line of sight as lens galaxies are functionally transparent to the H I signal.

Spectroscopic identification of lensing galaxies thus far has had a high rate of confirmation, e.g. Chan et al. (2016) reported a >70 per cent confirmation rate for a subset of 14 of the Holwerda et al. (2015) lens candidates. Similar numbers have been reported for SLACS (Bolton et al. 2006; Koopmans et al. 2006; Treu et al. 2006; Gavazzi et al. 2007). However, confirmation that these are strongly lensing galaxies may have to come from other means for these higher redshift candidate lenses. The resolution needed to resolve the characteristic arc of a gravitational lens in these cases is even better than *HST* (Fig. 8) but may be possible for ALMA or future observatories.

In practice, confirmation is more likely to come from using 21 cm emission line of H I. The lens galaxy is effectively transparent for the H I signal from the source, and it can be readily identified as it is separated in velocity space and the DEVILS spectroscopy provides a source redshift.

Lipnicky et al. (2018) reported the first strongly lensed H I detection, demonstrating this is a feasible approach. The DEVILS fields are all being targeted by intermediate and deep H I surveys.

Table 2. The DEVILS blended spectra in COSMOS (D10).

DEVILS ID	RA	Dec.	z_1	Template-1	z_2	Template-2	Classification	Notes
101919565	150.65279167	1.98026111	0.97	43	0.12	45	lens	
101919822	150.61966667	1.91290278	0.31	44	0.38	45	S-S	
101967337	150.54450000	2.02433333	0.06	46	0.87	45	lens	
102010304	150.66491667	2.24220278	0.12	44	0.98	45	S-E	
102010518	150.67683333	2.29440556	0.95	42	1.02	43	lens	
102186670	150.42608333	1.97702778	0.32	45	0.25	44	S	Single galaxy?
102187162	150.43245833	1.92986111	0.25	47	0.68	47	lens	
102187389	150.37729167	1.93966389	0.72	46	0.57	42	E	
102233089	150.46775000	2.06401667	0.55	42	0.43	45	S	Edge-on lens?
102233254	150.44391667	2.18347778	0.30	47	0.33	44	S-S	Distant edge-on
102233747	150.42983333	2.05285833	0.70	47	0.27	47	S-E	Tidal arc?
102234408	150.46829167	2.07676667	0.27	44	0.24	47	S-S	Big spiral in front
102280576	150.39179167	2.36102778	0.71	42	0.19	47	S-S	Distant edge-on spiral
102280688	150.42820833	2.37439444	0.27	45	0.22	47	S-E	ocg
102326921	150.42233333	2.59472222	0.77	47	0.00	46	S	Single
102327087	150.41666667	2.51389444	0.89	46	0.07	46	S-S	Small background galaxy
102327200	150.52104167	2.46149444	0.48	42	0.25	46	S-S	ocg
102418565	150.18912500	1.69931667	0.23	46	0.20	46	S	H II or very distant galaxy?
102465873	150.19379167	1.82101944	0.89	42	0.83	42	E-S	Ring galaxy?
102560691	150.21016667	2.31163611	0.75	46	0.30	47	S-S	Triple system interaction
102562458	150.32162500	2.27933333	0.25	45	0.89	42	S-E	Edge-on ocg
102609425	150.15820833	2.60825833	0.89	42	0.74	45	E-E	Quadruple+ system
102610080	150.13954167	2.59696667	0.72	45	0.28	47	S-S	Distant edge-on ocg
102705904	150.07375000	1.67840278	0.32	45	0.29	47	S-?	H II or distant galaxy
102753919	150.08550000	1.94860000	0.67	47	0.29	45	S-?	Big face-on spiral, no clear background
102754572	149.91062500	1.99146111	0.85	42	0.79	42	lens	
102755602	150.02570833	1.87035000	0.12	45	0.98	45	S	No bg galaxy
102801921	149.99262500	2.20221667	0.72	45	0.28	47	S-E	ocg
102849622	150.05612500	2.30426389	0.73	45	0.29	47	E/lens	Double nucleus? arc?
102849770	150.05479167	2.31726389	− 0.00	14	1.06	42	S	Face-on, no bg galaxy
102850336	149.98779167	2.31567500	0.93	40	0.82	42	S-E	Small bg galaxy
102850510	149.91050000	2.27933333	0.73	47	0.29	47	E	No clear bg galaxy
102852273	149.94070833	2.33096111	0.73	45	0.29	47	S	Large face-on spiral, no clear bg
102895172	150.04562500	2.57875833	0.74	46	0.30	47	S-S	ocg
102895353	150.03258333	2.50638333	0.29	46	0.73	45	lens	Faint arc?
102895479	150.05483333	2.44130278	0.73	45	0.29	46	S	Faint bg galaxy?
102940540	150.04470833	2.75957778	0.33	46	0.13	47	S-E	Interaction/ocg
102940702	150.04012500	2.75761944	0.63	46	0.21	47	S-S	Substructure or bg galaxy?
103084425	149.70545833	2.11458611	0.10	46	0.48	45	E	No sign of bg source
103087126	149.88595833	2.17616389	0.44	45	0.07	47	S-E	ocg, big face-on spiral
103131877	149.71279167	2.25295833	0.70	47	0.89	41	S	Substructure or bg galaxy?
103178590	149.82150000	2.44235556	0.23	47	0.65	47	E/lens	LSB ring?
103224426	149.77075000	2.78281944	0.51	40	0.28	46	E	No bg source
103225118	149.82491667	2.78900000	1.00	46	0.14	46	S-S	Multicomponent system
103225200	149.77250000	2.71349444	0.66	45	0.23	47	S	Big face-on spiral, bg source?
103274376	149.67195833	1.66864722	0.42	47	0.06	47	E	bg source close to nucleus?
103275225	149.52533333	1.75563889	0.75	47	0.30	47	E	Faint nearby companion
103275987	149.56145833	1.69020000	0.65	47	0.23	47	S-S	Multicomponent system
103323104	149.66395833	1.91104167	0.92	45	0.09	45	lens	Face-on ring spiral or lens?
103323224	149.58212500	1.88589444	0.63	47	0.21	47	S	Disturbed spiral
103323244	149.50720833	1.81979167	0.59	43	0.19	44	S-E	
103372556	149.66279167	2.10482500	0.63	47	0.22	47	S	bg or substructure
103374702	149.62220833	2.11793611	0.00	09	0.65	42	S	LSB Milky Way star contamination
103512791	149.54529167	2.76000556	0.27	42	0.30	44	E-S	Big elliptical, bg spirals
103513192	149.51020833	2.76900833	0.41	45	0.05	47	S-E	ocg
103513587	149.53975000	2.67549444	0.43	47	0.92	45	S-E	
103708094	149.45433333	2.44372500	0.61	46	0.31	45	–	

'ocg' means an occulting galaxy pair, which is good for measuring disc transparency at higher redshifts.

COSMOS is the focus of CHILES with the JVLA (Dodson et al. 2016; Fernández et al. 2016; Jones et al. 2016; Hess et al. 2019; Blue Bird et al. 2020). XMM-LSS is targeted with *L*-band observations for MIGHTEE (Jarvis et al. 2016; Delhaize et al. 2021; Maddox et al. 2021), and ECDF-S is the target for the *L*- and UHF-band observations for LADUMA (Holwerda 2011; Blyth 2015; Blyth et al. 2016; Baker et al. 2018). The H I disc of the source galaxy is much larger than the star-forming one, increasing the odds that a
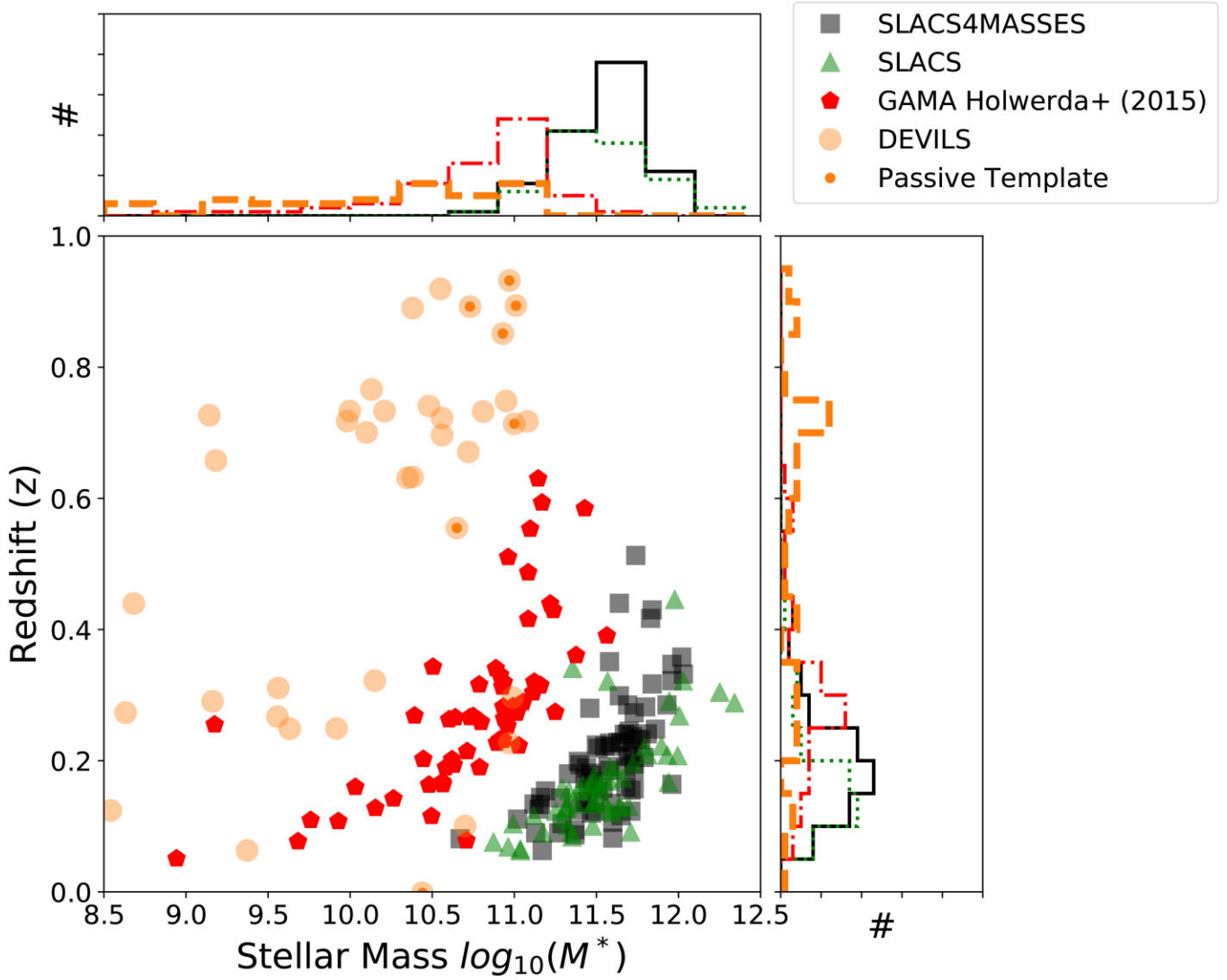
Figure 7. A comparison between spectroscopically identified strong lensing candidates. Stellar masses from Thorne et al. (2021) for the DEVILS/D10 candidates.
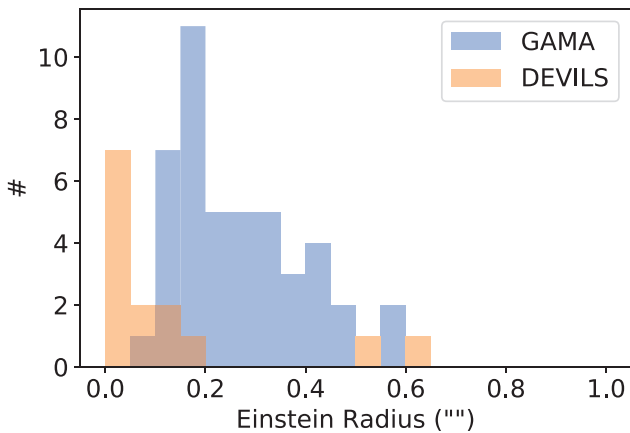

Figure 8. The histogram of predicted Einstein radii for the GAMA blended spectra from Holwerda et al. (2015) and those from the DEVILS DR1 catalogue (this paper).

magnified signal can be identified (see Deane et al. 2015). Starting from candidate selection using DEVILS and similar spectroscopy, the odds of detecting strongly lensed and therefore magnified H I from distant (i.e. $z > 0.1$ for H I) sources are set to increase significantly. Reporting the positions and redshifts of potential lensed H I sources for early H I follow-up was the main motivation for this paper.

The scientific use of such H I detections is to constrain the H I mass function (H I MF; Zwaan et al. 2005) at a higher redshift. At present, the H I content at higher redshifts is mostly measured from stacked H I spectra (Fabello et al. 2011, 2012; Delhaize et al. 2013; Maddox et al. 2013; Gereb et al. 2015; Bera et al. 2019; Chowdhury et al. 2020, 2021; Guo et al. 2020). With strongly lensed H I detections, and a reasonable prior for the magnification distribution, a wholly separate constraint can be given on the low-mass end of the H I MF.

In addition to the H I MF science, these gravitational lens candidates can be a useful cosmological probe. Increased numbers of strong gravitational lenses to monitor for supernovae in the source galaxy open the tantalizing possibility of time-delay cosmography (Treu & Marshall 2016; Oguri 2019). The possibility of the detection
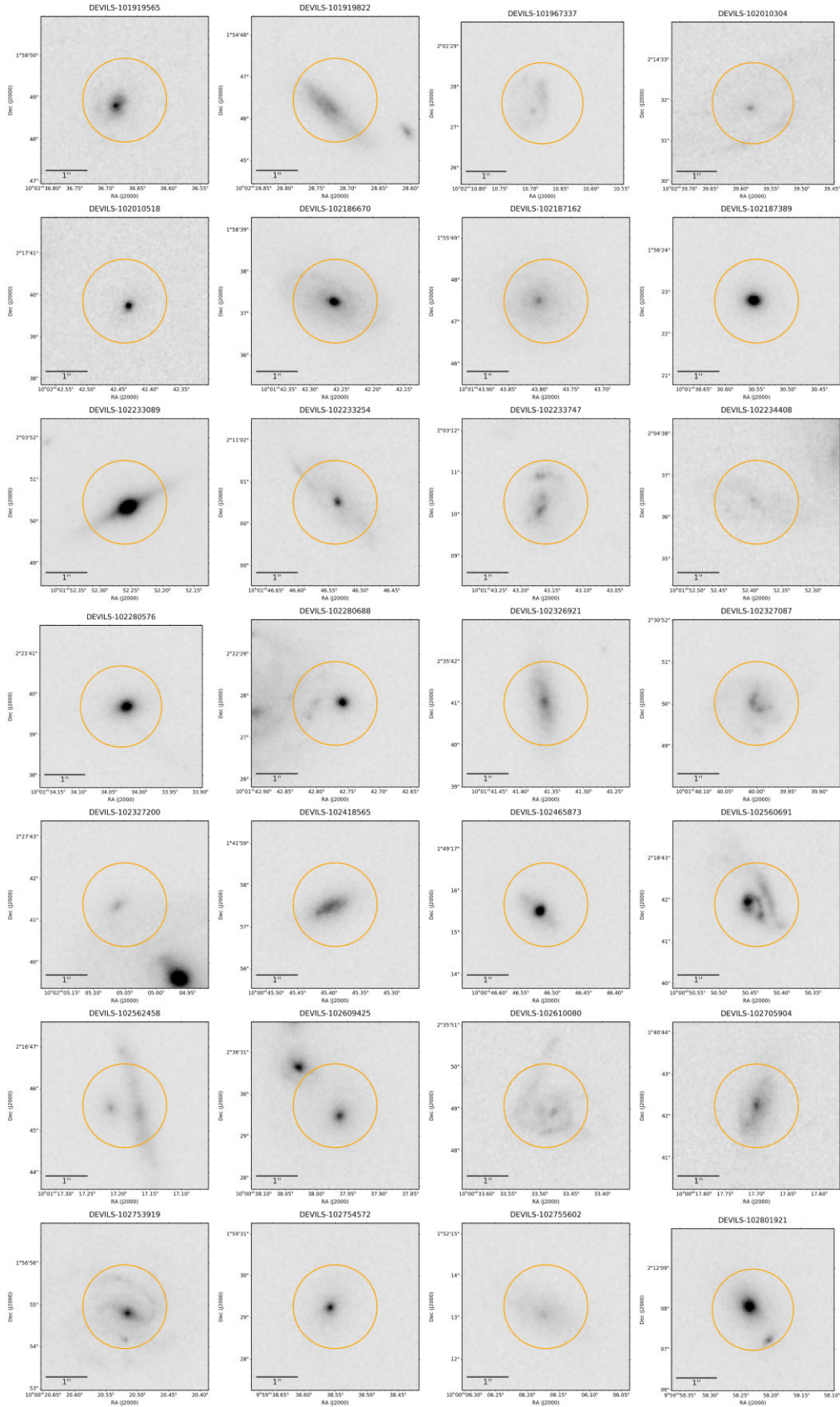
Figure 9. The cutouts from the *HST*/ACS COSMOS mosaic of all the blended spectra identified in DEVILS DR1. Pairs of galaxies along the line of sight are the most common blended spectra with passive elliptical systems that may be lensing a more distant source in the minority. Position of the DEVILS spectroscopic aperture is marked with an orange circle. Their spectra are shown in Fig. A1 of Appendix A.
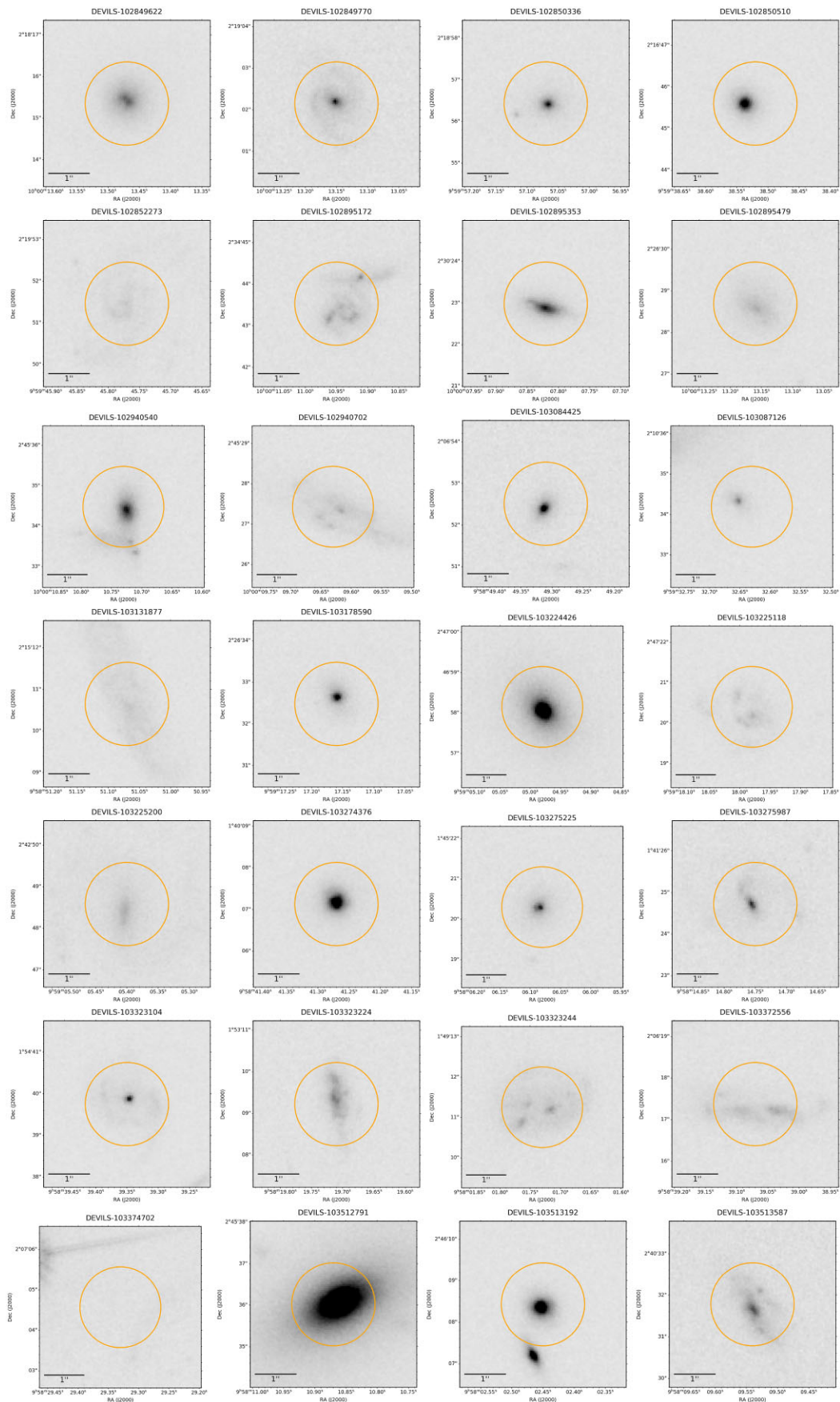
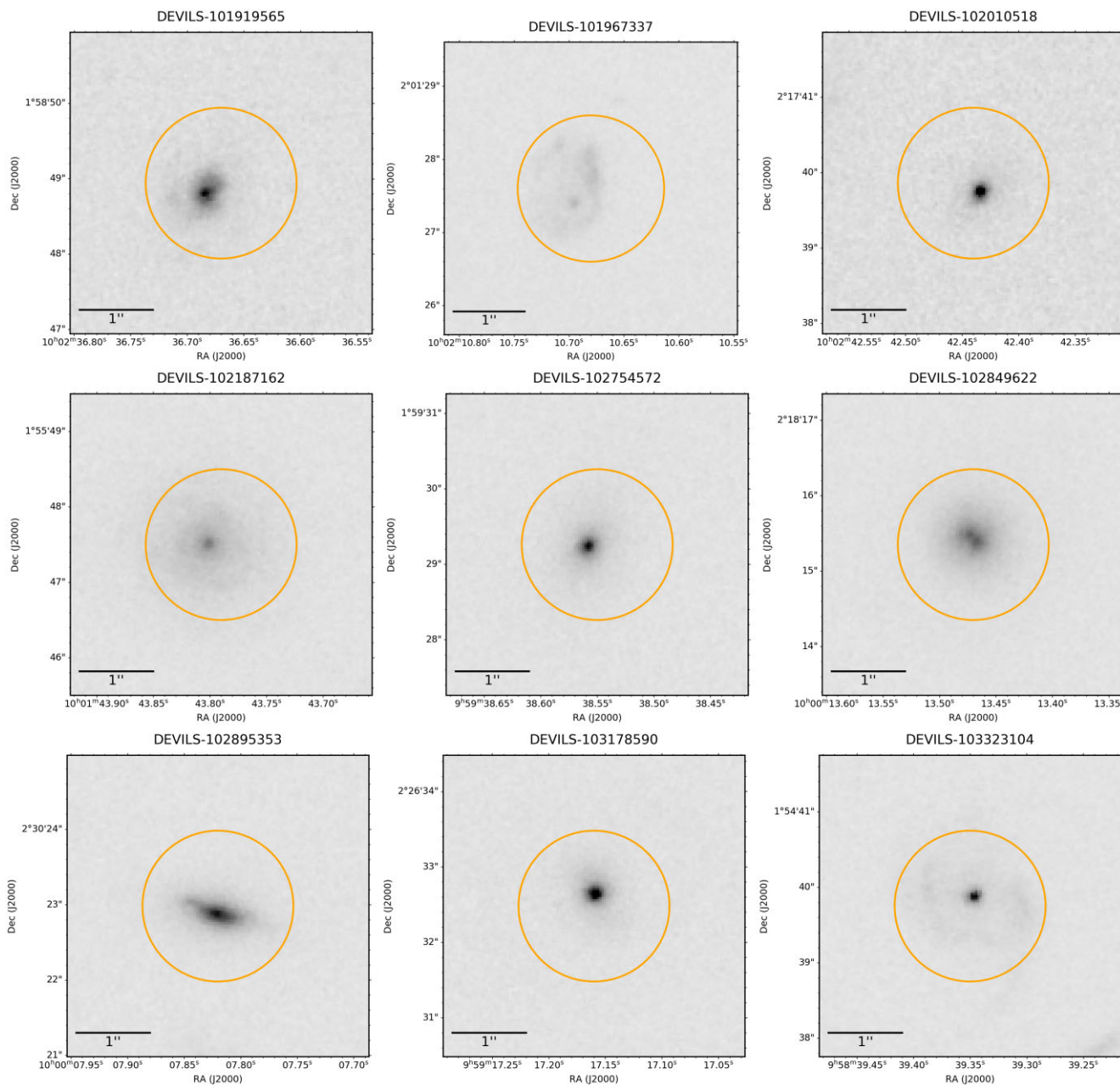**Figure 9** – *continued*

Figure 10. The candidate classical strong gravitational lenses in the DEVILS D10 sample, a massive elliptical with a more distant star-forming dwarf galaxy. In these COSMOS *F814W* images, it is difficult to identify source flux as it probes stellar continuum, not the star formation (e.g. rest-frame Hα) of the source galaxy.

of a strongly lensed supernova has long been considered to be a realistic prospect in statistical samples with modern survey cadence and sensitivity (Porciani & Madau 2000; Wang 2000; Holz 2001; Goobar et al. 2002a,b; Kostrzewa-Rutkowska, Wyrzykowski & Jaroszyński 2013). A few strongly lensed supernovae in galaxy–galaxy lenses have already been reported in iPTF, a precursor to the Zwicky Transient Factory (ZTF; Goobar et al. 2017), and in Pan-STARRS (Quimby et al. 2014). The most viable observational approach is to monitor a great number of suspected galaxy–galaxy lenses using near-future observatories, e.g. the *James Webb Space Telescope* (*JWST*; Petrushevska et al. 2018), the Vera C. Rubin Observatory (Liao 2019; Tu, Hu & Wang 2019), and ZTF (Shu et al. 2018; Goldstein et al. 2019).

A few well-characterized lenses can make a significant difference in cosmography to determine the expansion rate of the Universe.

For example, the H0LICOW[3] project has monitored *four* strong gravitational lenses with a quasar behind it for some time (cf. Suyu et al. 2017; Birrer et al. 2019) and constrained the expansion rate independently of the other two measurements, Type Ia supernova distances ($H_0 = 73$ km s^{-1} Mpc^{-1}; Beaton et al. 2016; Riess et al. 2016, 2018; Riess 2019) and the cosmic microwave background ($H_0 = 68$ km s^{-1} Mpc^{-1}; Planck Collaboration 2020). The H0LICOW result has not yet broken the current tension between the two values for H_0, but this approach shows great promise. Quasars do change over time but much less predictably than supernovae. With a few lensed sources and more reliable timing, lensed supernovae offer a very attractive alternative for cosmography. Strongly lensing

---

[3]H0 Lenses in COSMOGRAIL's Wellspring (Suyu et al. 2017).

candidates at higher redshifts, even without resolved imaging, may offer additional constraints.

Many of the new DEVILS candidate lenses are at greater distances offering a longer expected time delay, which is a function of the lens and source distances. Presently, time-delay supernovae are limited to a lower redshift (e.g. $z < 0.1$; Quimby et al. 2014; Goobar et al. 2017). The longer expected time delay offers the option to measure the Hubble constant (H_0) from the multiple imaged supernova more accurately. The multiple images need not be resolved, but each light curve does need to be resolved in the time series. With a time delay of the order of weeks, a supernova light curve could easily be modelled for each event, allowing for a greater relative accuracy of the delay and hence inferred Hubble expansion rate. Each DEVILS target field is also a Vera C. Rubin Observatory deep drilling field, and the LADUMA target field (CDF-S) is in the THUNDERKAT (Fender et al. 2016) transient search, in conjunction with the MeerLicht optical transient searches (Hosenie et al. 2021; Woudt 2021). The emphasis on transient searches in these fields makes candidate strong gravitational lenses in them especially attractive for the topic of cosmography.

The next generation of spectroscopic surveys is being planned with the 4MOST instrument (de Jong et al. 2012; Depagne 2015). Planned extragalactic surveys are the two-tiered Wide Area Vista Extragalactic Survey (WAVES; Driver et al. 2019), the Optical, Radio Continuum and H I Deep Spectroscopic Survey (ORCHIDSS; Duncan et al., in preparation), and a cosmological low-S/N wide-area survey (CRS; Richard et al. 2019). These 4MOST surveys are expected to achieve high completeness in their target fields and yield a boon of spectroscopically confirmed strong lensing systems, especially those with more distant lenses and lower masses.

Strong gravitational lenses will continue to be identified in future spectroscopic surveys, e.g. WAVES and ORCHIDSS using the 4MOST instrument. Confirmation of these lenses may come in the form of magnified H I rather (cf. Deane et al. 2015; Blecher et al. 2019) than resolved imaging of the lensing arcs or high-resolution imaging even with the *Roman* or *Euclid* space telescopes or targeted follow-up with *JWST*. Future data releases from DEVILS promise to improve the numbers of strong lenses known at $z \sim 1$ in the immediate future.

ACKNOWLEDGEMENTS

This research made use of APLPY, an open-source plotting package for PYTHON hosted at http://aplpy.github.com. This research also made use of ASTROPY, a community-developed core PYTHON package for astronomy (Astropy Collaboration et al. 2013, 2018).

DATA AVAILABILITY STATEMENT

DEVILS DR1 will be made available with a separate publication via the project website.[4] Relevant blended spectrum information will be part of the full DR1 as well as listed in the tables of this paper.

[4] https://devilsurvey.org/wp/

REFERENCES

Astropy Collaboration et al., 2013, A&A, 558, A33
Astropy Collaboration et al., 2018, AJ, 156, 123
Auger M. W., Treu T., Bolton A. S., Gavazzi R., Koopmans L. V. E., Marshall P. J., Bundy K., Moustakas L. A., 2009, ApJ, 705, 1099
Auger M. W., Treu T., Bolton A. S., Gavazzi R., Koopmans L. V. E., Marshall P. J., Moustakas L. A., Burles S., 2010, ApJ, 724, 511
Baker A. J., Blyth S., Holwerda B. W., LADUMA team, 2018, American Astronomical Society Meeting Abstracts #231. p. 231.07
Baldry I. K. et al., 2014, MNRAS, 441, 2440
Beaton R. L. et al., 2016, ApJ, 832, 210
Bera A., Kanekar N., Chengalur J. N., Bagla J. S., 2019, ApJ, 882, L7
Birrer S. et al., 2019, MNRAS, 484, 4726
Blecher T., Deane R., Heywood I., Obreschkow D., 2019, MNRAS, 484, 3681
Blue Bird J. et al., 2020, MNRAS, 492, 153
Blyth S., 2015, Proc. SALT Science Conference 2015 (SSC2015). Stellenbosch Institute of Advanced Study, South Africa, p. 36
Blyth S. et al., 2016, in Proc. MeerKAT Science: On the Pathway to the SKA (MeerKAT2016). Stellenbosch, South Africa, p. 4
Bolton A. S., Burles S., Koopmans L. V. E., Treu T., Moustakas L. A., 2006, ApJ, 638, 703
Bolton A. S., Burles S., Koopmans L. V. E., Treu T., Gavazzi R., Moustakas L. A., Wayth R., Schlegel D. J., 2008a, ApJ, 682, 964
Bolton A. S., Treu T., Koopmans L. V. E., Gavazzi R., Moustakas L. A., Burles S., Schlegel D. J., Wayth R., 2008b, ApJ, 684, 248
Chan J. H. H. et al., 2016, ApJ, 832, 135
Chang C. et al., 2015, ApJ, 801, 73
Chowdhury A., Kanekar N., Chengalur J. N., Sethi S., Dwarakanath K. S., 2020, Nature, 586, 369
Chowdhury A., Kanekar N., Das B., Dwarakanath K. S., Sethi S., 2021, ApJ, 913, L24
Collett T. E., 2015, ApJ, 811, 20
Collett T. E., 2017, Astrophysics Source Code Library, record ascl:1705.009
Collett T. E. et al., 2018, Science, 360, 1342
Collier W. P., Smith R. J., Lucey J. R., 2018a, MNRAS, 473, 1103
Collier W. P., Smith R. J., Lucey J. R., 2018b, MNRAS, 478, 1595
Cyr-Racine F.-Y., Keeton C. R., Moustakas L. A., 2019, Phys. Rev. D, 100, 023013
Davies L. J. M. et al., 2018, MNRAS, 480, 768
de Blok W. J. G. et al., 2020, A&A, 643, A147
de Jong R. S. et al., 2012, in McLean I. S., Ramsay S. K., Takami H., eds, Proc. SPIE Conf. Ser. Vol. 8446, Ground-based and Airborne Instrumentation for Astronomy IV. SPIE, Bellingham, p. 84460T
Deane R. P., Obreschkow D., Heywood I., 2015, MNRAS, 452, L49
Delhaize J., Meyer M. J., Staveley-Smith L., Boyle B. J., 2013, MNRAS, 433, 1398
Delhaize J. et al., 2021, MNRAS, 501, 3833
Depagne É., 2015, in Miglio A., Girardi L., Eggenberger P., Montalban J., eds, Asteroseismology of Stellar Populations in the Milky Way. Springer International Publishing, Switzerland, p. 147
Dobler G., Keeton C. R., Bolton A. S., Burles S., 2008, ApJ, 685, 57
Dodson R. et al., 2016, A&C, 14, 8
Domingue D. L., Keel W. C., Ryder S. D., White R. E., III, 1999a, AJ, 118, 1542
Domingue D. L., Keel W. C., White R. E., Ryder S. D., 1999b, American Astronomical Society Meeting. p. 0704
Domingue D. L., Keel W. C., White R. E., III, 2000, ApJ, 545, 171
Driver S. P. et al., 2009, Astron. Geophys., 50, 050000
Driver S. P. et al., 2019, The Messenger, 175, 46
Fabello S., Kauffmann G., Catinella B., Giovanelli R., Haynes M. P., Heckman T. M., Schiminovich D., 2011, MNRAS, 416, 1739
Fabello S., Kauffmann G., Catinella B., Li C., Giovanelli R., Haynes M. P., 2012, MNRAS, 427, 2841
Fender R. et al., 2016, Proceedings of MeerKAT Science: On the Pathway to the SKA (MeerKAT2016). Stellenbosch, South Africa, p. 13
Fernández X. et al., 2016, ApJ, 824, L1

Gavazzi R., Treu T., Rhodes J. D., Koopmans L. V. E., Bolton A. S., Burles S., Massey R. J., Moustakas L. A., 2007, ApJ, 667, 176

Gereb K., Morganti R., Oosterloo T. A., Hoppmann L., Staveley-Smith L., 2015, A&A, 580, A43

Goldstein D. A., Nugent P. E., Goobar A., 2019, ApJS, 243, 6

Goobar A., Mörtsell E., Amanullah R., Goliath M., Bergström L., Dahlén T., 2002a, A&A, 392, 757

Goobar A., Mörtsell E., Amanullah R., Nugent P., 2002b, A&A, 393, 25

Goobar A. et al., 2017, Science, 356, 291

Guo H., Jones M. G., Haynes M. P., Fu J., 2020, ApJ, 894, 92

Healy J. et al., 2021, A&A, 650, A76

Hess K. M. et al., 2019, MNRAS, 484, 2234

Holwerda B. W., ed., 2011, Am. Astron. Soc. Meeting Abstr. 217, 133.17

Holwerda B. W., Keel W. C., 2013, A&A, 556, A42

Holwerda B. W., Keel W. C., 2016, IAUFM, 29B, 173

Holwerda B. W., Keel W. C., 2017, IAUS, 321, 248

Holwerda B. W., Keel W. C., Bolton A., 2007, AJ, 134, 2385

Holwerda B. W., Keel W. C., Williams B., Dalcanton J. J., de Jong R. S., 2009, AJ, 137, 3000

Holwerda B. W., Böker T., Dalcanton J. J., Keel W. C., de Jong R. S., 2013, MNRAS, 433, 47

Holwerda B. W. et al., 2015, MNRAS, 449, 4277

Holwerda B. W., Knabel S., Steele R. C., Strolger L., Kielkopf J., Jacques A., Roemer W., 2021, MNRAS, 505, 1316

Holz D. E., 2001, ApJ, 556, L71

Hosenie Z. et al., 2021, Exp. Astron. Experimental Astronomy, p. 15

Huang X. et al., 2020, ApJ, 894, 78

Jacobs C. et al., 2019, ApJS, 243, 17

Jarvis M. J. et al., 2013, MNRAS, 428, 1281

Jarvis M. et al., 2016, in Proc. MeerKAT Science: On the Pathway to the SKA (MeerKAT2016). Stellenbosch, South Africa. p. 6

Johnston S. et al., 2008, Exp. Astron., 22, 151

Jones M. G., Haynes M. P., Giovanelli R., Papastergis E., 2016, MNRAS, 455, 1574

Keel W. C., White R. E., III, 2001a, AJ, 121, 1442

Keel W. C., White R. E., III, 2001b, AJ, 122, 1369

Knabel S. et al., 2020, AJ, 160, 223

Koopmans L. V. E., Treu T., Bolton A. S., Burles S., Moustakas L. A., 2006, ApJ, 649, 599

Koribalski B. S. et al., 2020, Ap&SS, 365, 118

Kostrzewa-Rutkowska Z., Wyrzykowski Ł., Jaroszyński M., 2013, MNRAS, 429, 2392

Lee C.-H., 2017, Res. Notes Am. Astron. Soc., 1, 12

Li R. et al., 2020, ApJ, 899, 30

Liao K., 2019, ApJ, 871, 113

Lipnicky A. et al., 2018, MNRAS, 476, 3097

Liske J. et al., 2015, MNRAS, 452, 2087

McCracken H. J. et al., 2012, A&A, 544, A156

Maddox N., Hess K. M., Blyth S. L., Jarvis M. J., 2013, MNRAS, 433, 2613

Maddox N. et al., 2021, A&A, 646, A35

Mason C. A. et al., 2015, ApJ, 805, 79

Oguri M., 2010, PASJ, 62, 1017

Oguri M., 2019, Rep. Prog. Phys., 82, 126901

Petrillo C. E. et al., 2017, MNRAS, 472, 1129

Petrillo C. E. et al., 2019a, MNRAS, 482, 807

Petrillo C. E. et al., 2019b, MNRAS, 484, 3879

Petrushevska T., Okamura T., Kawamata R., Hangard L., Mahler G., Goobar A., 2018, Astron. Rep., 62, 917

Planck Collaboration, 2014, A&A, 571, A16

Planck Collaboration, 2020, A&A, 641, A6

Porciani C., Madau P., 2000, ApJ, 532, 679

Quimby R. M. et al., 2014, Science, 344, 396

Richard J. et al., 2019, The Messenger, 175, 50

Riess A. G., 2019, Nat. Rev. Phys., 2, 10

Riess A. G. et al., 2016, ApJ, 826, 56

Riess A. G. et al., 2018, ApJ, 853, 126

Robotham A. S. G., Davies L. J. M., Driver S. P., Koushan S., Taranu D. S., Casura S., Liske J., 2018, MNRAS, 476, 3137

Robotham A. S. G., Bellstedt S., Lagos C. d. P., Thorne J. E., Davies L. J., Driver S. P., Bravo M., 2020, MNRAS, 495, 905

Scoville N. et al., 2007, ApJS, 172, 38

Sharp R. et al., 2006, in McLean I. S. Iye M., eds. Proceedings of the SPIE, Volume 6269. Astronomical Telescopes and Instrumentation, Orlando, Florida, USA, p. 13

Shu Y. et al., 2015, ApJ, 803, 71

Shu Y. et al., 2017, ApJ, 851, 48

Shu Y., Bolton A. S., Mao S., Kang X., Li G., Soraisam M., 2018, ApJ, 864, 91

Smith R. J., 2017, MNRAS, 464, L46

Smith R. J., Collier W. P., Ozaki S., Lucey J. R., 2020, MNRAS, 493, L33

Suyu S. H. et al., 2017, MNRAS, 468, 2590

Talbot M. S. et al., 2018, MNRAS, 477, 195

Thorne J. E. et al., 2021, MNRAS, 505, 540

Tortora C., Koopmans L. V. E., Napolitano N. R., Valentijn E. A., 2018, MNRAS, 473, 2324

Treu T., Marshall P. J., 2016, A&AR, 24, 11

Treu T., Koopmans L. V., Bolton A. S., Burles S., Moustakas L. A., 2006, ApJ, 640, 662

Treu T., Gavazzi R., Gorecki A., Marshall P. J., Koopmans L. V. E., Bolton A. S., Moustakas L. A., Burles S., 2009, ApJ, 690, 670

Tu Z. L., Hu J., Wang F. Y., 2019, MNRAS, 484, 4337

Verlinde E., 2017, SciPost Phys., 2, 016

Wang Y., 2000, ApJ, 531, 676

Wang J. et al., 2021, ApJ, 915, 70

White R. E., III, Keel W. C., Conselice C. J., 2000, ApJ, 542, 761

Wojtak R., Hjorth J., Gall C., 2019, MNRAS, 487, 3342

Woudt P., 2021, in AFAS2 2021: Conference of the African Astronomical Society, held 8-12 March. p. 35

Zwaan M. A., Meyer M. J., Staveley-Smith L., Webster R. L., 2005, MNRAS, 359, L30

APPENDIX A: BLENDED SPECTRA IN DEVILS

In this appendix, we list the DEVILS object flagged as candidate blended spectra, listing their positions and redshifts in two additional tables, one for XMM-LSS (D02), Table A1, and one for ECDF-S (D03), Table A2. We show the spectra for the candidates in the COSMOS (D10) field listed in Table 2 with the spectra shifted to the rest-frame wavelength for both redshift solutions in Fig. 5.

Table A1. The DEVILS blended spectra in XMM-LSS (D02).

DEVILS ID	RA	Dec.	z_1	Template-1	z_2	Template-2
23945817	35.50616667	− 4.54419722	0.95	43	1.02	43
23995608	35.48341667	− 4.33065000	0.76	47	0.00	45
23996308	35.46912500	− 4.21832500	0.70	45	0.27	46
24041251	35.37587500	− 5.07945833	0.38	47	0.27	44
24142011	35.24208333	− 4.51141389	0.79	46	0.01	46
24143221	35.21520833	− 4.59569444	0.27	46	0.30	46
24193078	35.24100000	− 4.38532500	0.46	45	0.08	47
24241442	34.98895833	− 5.11926667	0.62	47	0.20	47
24241567	34.96800000	− 5.15127222	0.25	44	0.22	47
24242039	35.03679167	− 4.99350833	0.14	45	1.00	45
24242215	35.06750000	− 5.16637500	0.63	46	0.21	47
24293199	35.08458333	− 4.94779167	0.27	44	0.30	47
24293268	35.01629167	− 4.71430556	0.25	44	0.26	47
24293310	35.12950000	− 4.70440556	0.74	45	0.29	46
24293967	34.98733333	− 4.90861111	0.82	45	0.03	47
24294352	35.15616667	− 4.87894167	0.75	47	0.30	47
24345222	35.02795833	− 4.61946944	0.63	41	0.24	47
24345466	35.02870833	− 4.63459444	0.77	45	0.00	45
24345663	35.17904167	− 4.66834444	0.95	43	1.02	43
24394824	35.09225000	− 4.27165833	0.60	42	− 4.71	12
24395213	35.18966667	− 4.27158889	0.48	45	0.10	47
24440571	34.84237500	− 5.08841389	0.31	47	0.28	47
24442735	34.88283333	− 5.10223056	0.71	47	0.27	47
24491257	34.95154167	− 4.90585833	0.76	47	0.31	47
24491480	34.87079167	− 4.86123611	0.31	44	0.27	47
24491527	34.93812500	− 4.86090556	0.28	46	0.72	47
24491585	34.92358333	− 4.74284444	0.75	46	0.30	47
24491650	34.90016667	− 4.80743333	0.65	45	0.23	47
24491864	34.76579167	− 4.79886389	0.33	45	0.30	47
24491889	34.85179167	− 4.84960833	0.71	47	0.27	47
24492071	34.95025000	− 4.85865833	0.82	42	0.04	45
24492650	34.91337500	− 4.89559167	0.21	46	0.62	45
24492762	34.73716667	− 4.75255278	0.89	46	0.07	46
24544023	34.79745833	− 4.53279167	0.03	46	0.81	43
24544177	34.88254167	− 4.46093611	0.33	47	0.33	47
24596487	34.86800000	− 4.31477778	0.75	41	0.04	47
24596709	34.83625000	− 4.26286667	0.44	47	0.07	47
24596900	34.96254167	− 4.21835000	0.69	47	0.26	47
24640004	34.60112500	− 4.99404167	0.71	47	0.81	41
24640069	34.63387500	− 5.01778889	0.65	47	0.87	40
24690693	34.49441667	− 4.81551111	0.71	45	0.28	47
24690952	34.51208333	− 4.89002778	0.75	45	0.30	47
24691156	34.63895833	− 4.75832500	0.71	47	0.27	47
24692379	34.62654167	− 4.79908333	0.72	45	0.28	47
24740073	34.65158333	− 4.45387778	0.79	47	0.02	44
24837980	34.28087500	− 5.15114167	0.20	45	1.12	45
24838186	34.37887500	− 5.02776389	0.80	47	0.02	44
24838207	34.24262500	− 5.06420000	0.25	47	0.68	45
24838544	34.46829167	− 5.09759167	0.62	40	0.53	44
24942850	34.37150000	− 4.63441111	0.71	47	0.27	47
24943476	34.28445833	− 4.58350833	0.21	45	0.18	47
24992849	34.46066667	− 4.28522778	0.74	47	0.45	45
24992987	34.38341667	− 4.40945278	0.43	47	0.07	47
24993238	34.29933333	− 4.28556389	0.15	45	0.16	47
24993260	34.33441667	− 4.38700833	0.83	47	0.04	47
24993840	34.33962500	− 4.40013611	0.25	47	0.68	45
25039757	34.22391667	− 5.11365278	0.39	47	0.71	46
25039908	34.21112500	− 5.13786667	0.67	47	0.25	45
25040091	34.03766667	− 4.97813611	0.48	45	0.10	47
25040892	34.09312500	− 5.06527778	0.14	45	1.01	45
25108384	34.00550000	− 4.81034167	0.64	45	0.38	46
25108806	34.16625000	− 4.73569444	0.71	45	0.27	46
25108841	34.21095833	− 4.82175556	0.36	47	0.01	47
25109419	34.17883333	− 4.69961667	0.30	47	0.74	45
25109652	34.11029167	− 4.92928611	0.46	46	0.08	47

Table A1 – *continued*

DEVILS ID	RA	Dec.	z_1	Template-1	z_2	Template-2
25175636	34.11670833	− 4.46486944	0.72	43	0.69	40
25176091	34.01475000	− 4.55083056	0.50	47	0.12	47
25176779	34.17937500	− 4.53499722	0.75	47	0.30	46
25241942	34.19083333	− 4.35923611	0.42	42	0.25	47
25242440	34.18587500	− 4.26509167	0.35	40	9.11	12
25242758	34.06904167	− 4.29557778	0.72	47	0.28	47
25242789	34.19308333	− 4.23933056	0.43	47	0.09	46
25243097	34.08058333	− 4.40158056	0.14	47	0.49	45
25243428	34.17683333	− 4.32388333	0.45	47	0.08	47
25243492	34.07950000	− 4.28745000	0.45	47	0.07	47

Table A2. The DEVILS blended spectra in ECDF-S (D03).

| DEVILS ID	RA	Dec.	z_1	Template-1	z_2	Template-2
31364972	53.89120833	− 27.76997222	0.95	42	1.02	43
31366150	53.77891667	− 27.95961944	0.63	45	0.00	22
31420864	53.85745833	− 27.67635556	0.20	44	0.00	47
31470431	53.53220833	− 28.35941944	0.31	47	− 2.40	09
31470803	53.55166667	− 28.44153889	0.08	47	0.65	42
31472266	53.58391667	− 28.37151944	0.71	47	0.27	47
31580189	53.54012500	− 27.90944444	0.10	44	0.41	42
31580674	53.71579167	− 27.82735556	0.61	47	0.19	47
31580973	53.63183333	− 27.77484722	0.47	47	0.92	45
31581136	53.60870833	− 27.83990833	0.74	47	0.30	47
31581150	53.62883333	− 27.90129722	0.40	46	0.88	45
31581359	53.56654167	− 27.78446389	0.67	45	0.24	46
31585572	53.43470833	− 27.87049167	0.73	45	0.29	47
31635177	53.49095833	− 27.60029722	0.77	45	0.01	44
31635948	53.57295833	− 27.57112222	0.78	46	0.01	43
31737748	53.30095833	− 28.02351111	0.29	47	0.73	45
31738799	53.14987500	− 28.05283611	0.21	46	0.63	47
31739322	53.19358333	− 28.00018889	0.28	47	0.73	45
31897468	52.86245833	− 28.30308056	0.28	47	0.73	47
31897890	52.93775000	− 28.32748333	0.71	47	0.28	47
31898084	52.84445833	− 28.40419167	0.86	40	0.79	47
31898601	53.08812500	− 28.25800556	0.77	45	0.01	45
31898627	52.97508333	− 28.30872500	0.64	47	0.22	47
31898958	53.05341667	− 28.34696111	0.71	47	0.28	47
31899017	52.92825000	− 28.41990278	0.28	47	0.72	45
31953454	52.84104167	− 28.15541389	0.62	45	0.21	47
31953908	52.88858333	− 28.09198611	0.00	13	0.36	47
31954005	53.05487500	− 28.20985556	1.03	43	0.15	45
32008128	52.80141667	− 27.83991111	0.28	44	0.25	46
32064222	52.86333333	− 27.70248333	0.57	46	0.48	41
32064590	53.00425000	− 27.55768333	0.73	47	0.29	47
32064684	53.06500000	− 27.51943889	0.58	45	0.18	47
32064950	52.79958333	− 27.66902222	0.31	44	0.28	46
32065013	53.00483333	− 27.55390556	0.73	47	0.29	47
32115739	52.64220833	− 28.26730833	0.32	45	0.77	45
32115855	52.71337500	− 28.28865278	0.75	47	0.30	46
32116509	52.79425000	− 28.32276667	0.68	47	0.25	44
32170820	52.74045833	− 28.09380000	0.49	47	0.11	46
32171195	52.76537500	− 28.03151389	0.66	41	0.30	44
32172424	52.66054167	− 28.11606111	0.74	45	0.29	47
32172833	52.76887500	− 28.09402222	0.93	45	0.10	43
32227404	52.48862500	− 27.77536667	0.74	45	0.30	47
32227786	52.58745833	− 27.82791389	0.28	47	0.73	45
32227924	52.68816667	− 27.78745833	0.79	45	0.01	47
32228358	52.62358333	− 27.84935556	0.30	46	0.74	46
32283863	52.72366667	− 27.60104722	0.65	46	0.23	47
32283912	52.63470833	− 27.64496944	− 0.00	44	0.76	45
32283973	52.79820833	− 27.52830556	0.12	46	0.23	46
32377963	52.40470833	− 28.24047222	0.76	40	0.28	44
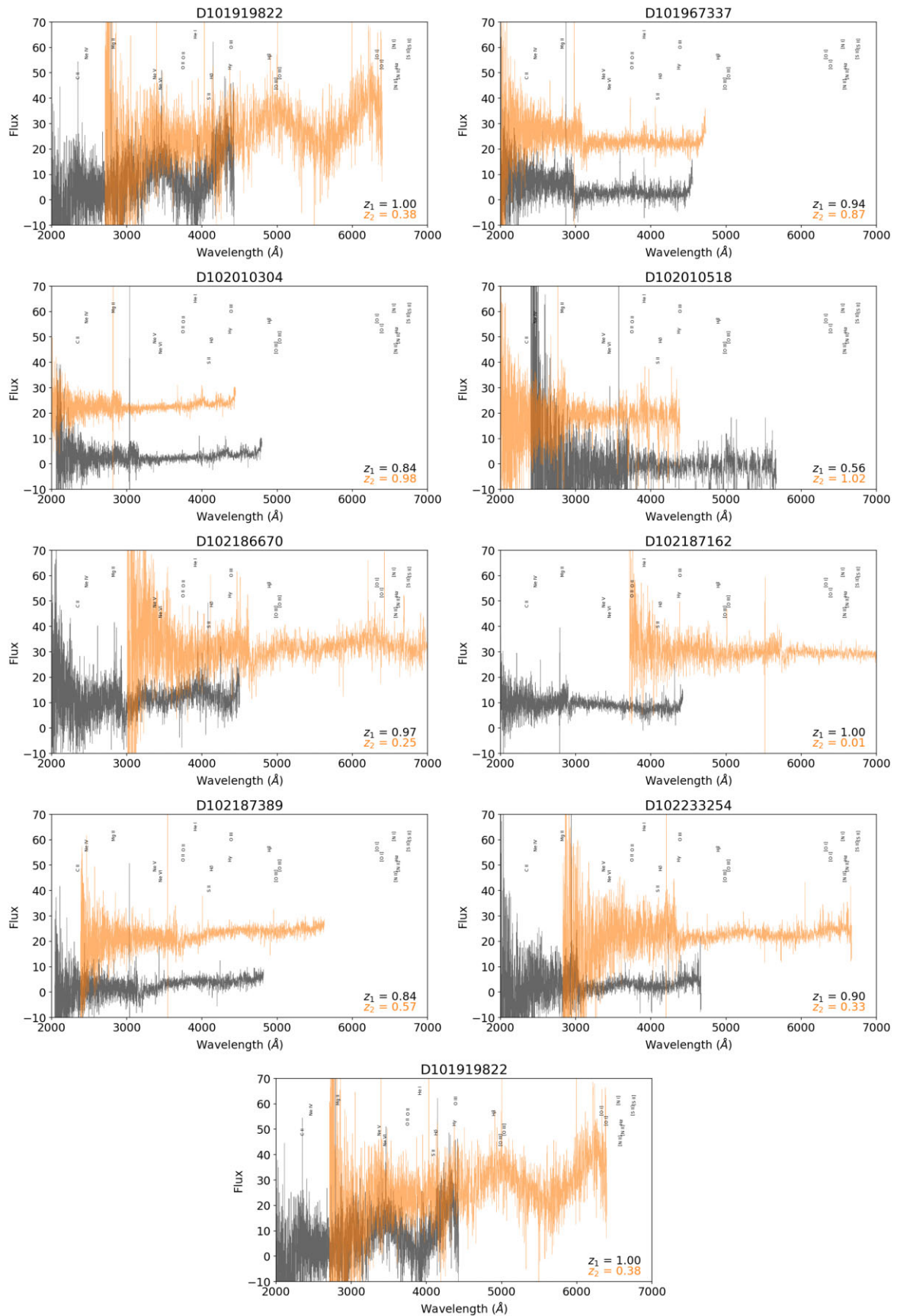
Figure A1. DEVILS spectra identified as blens by the cross-correlation parameters from AUTOZ. Emission and absorption features are shown at their restframe wavelengths with the spectrum moved to the first (black) and second (orange) redshift solution.
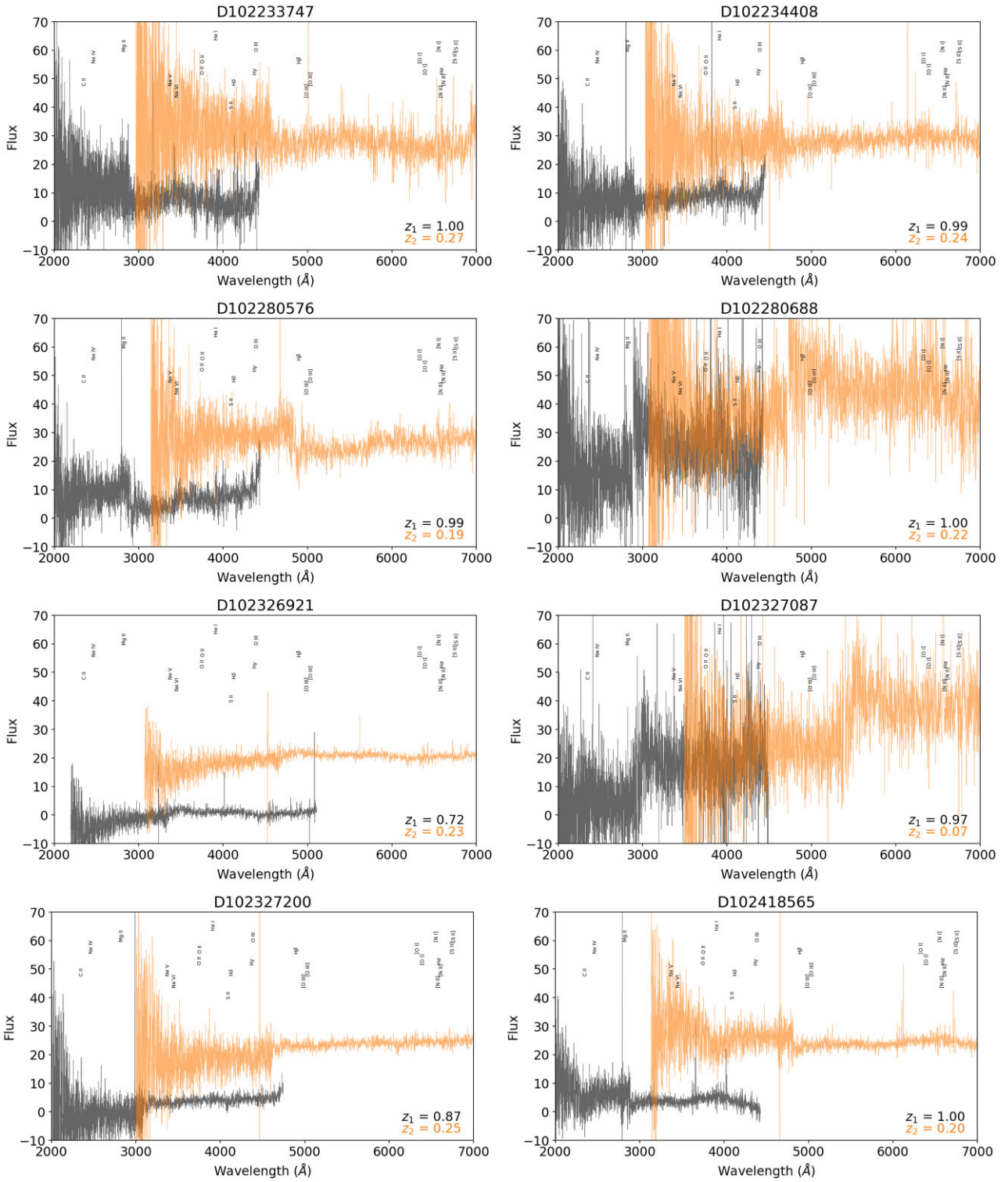
Figure A1 *– continued*
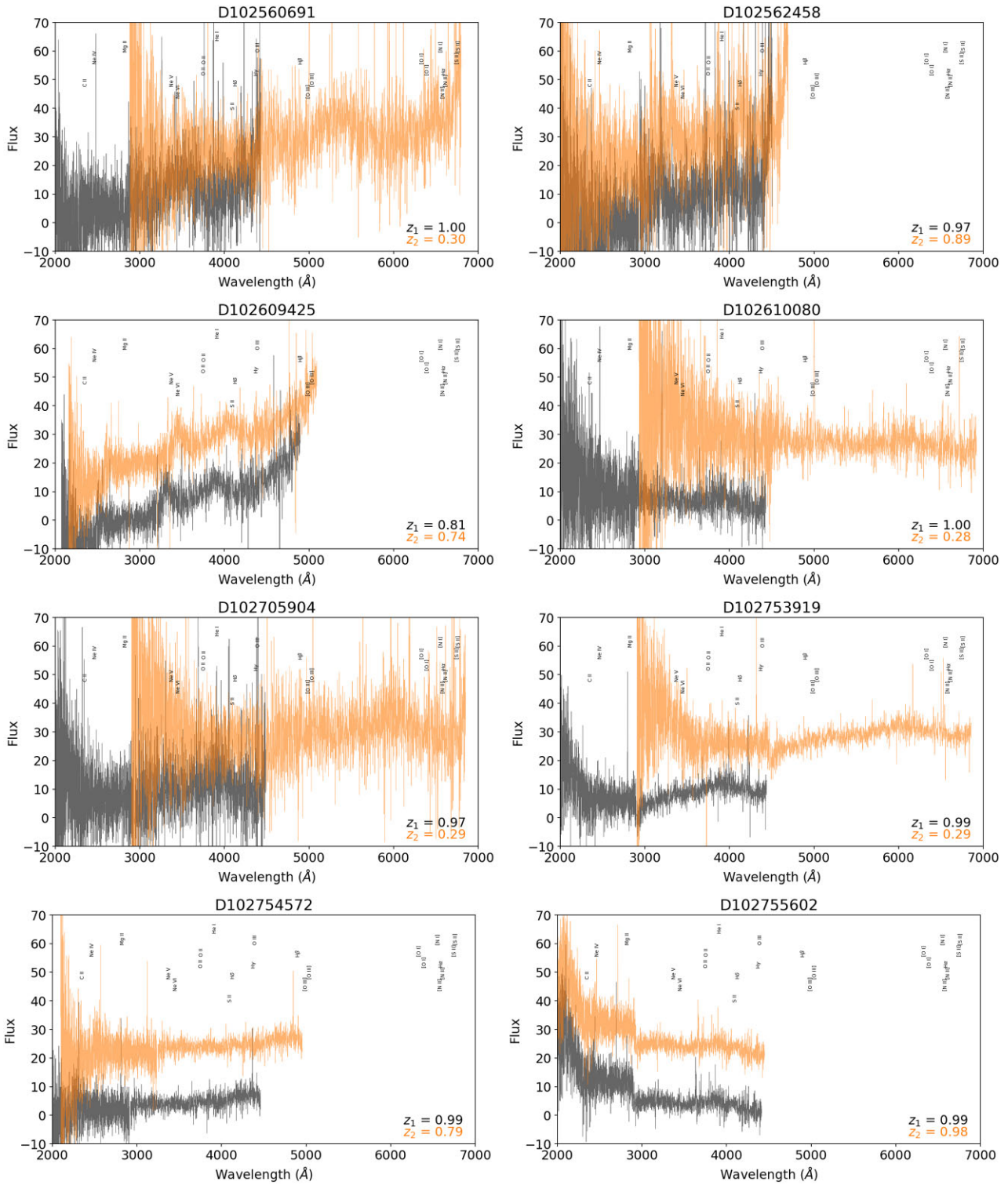
Figure A1 – *continued*
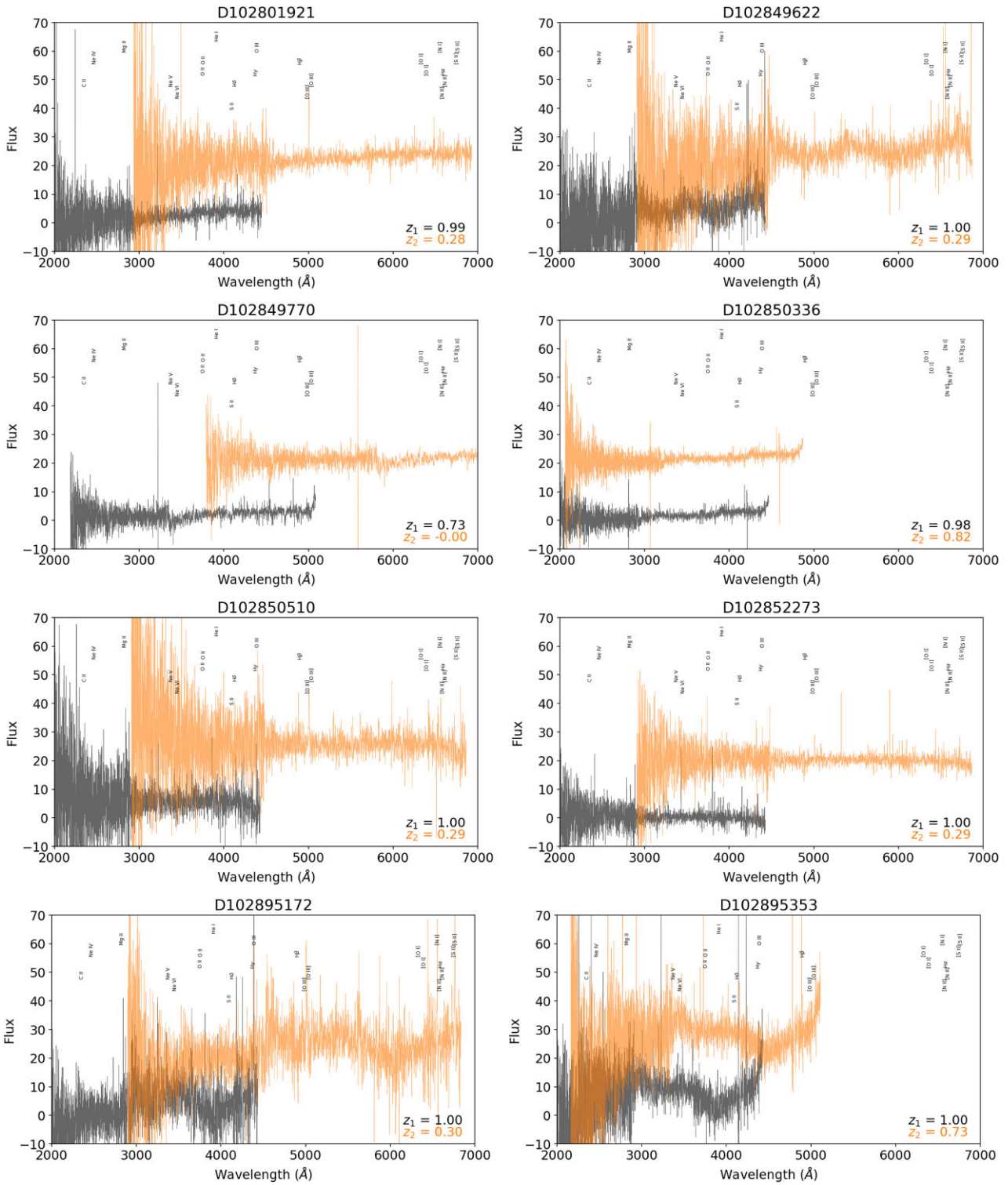
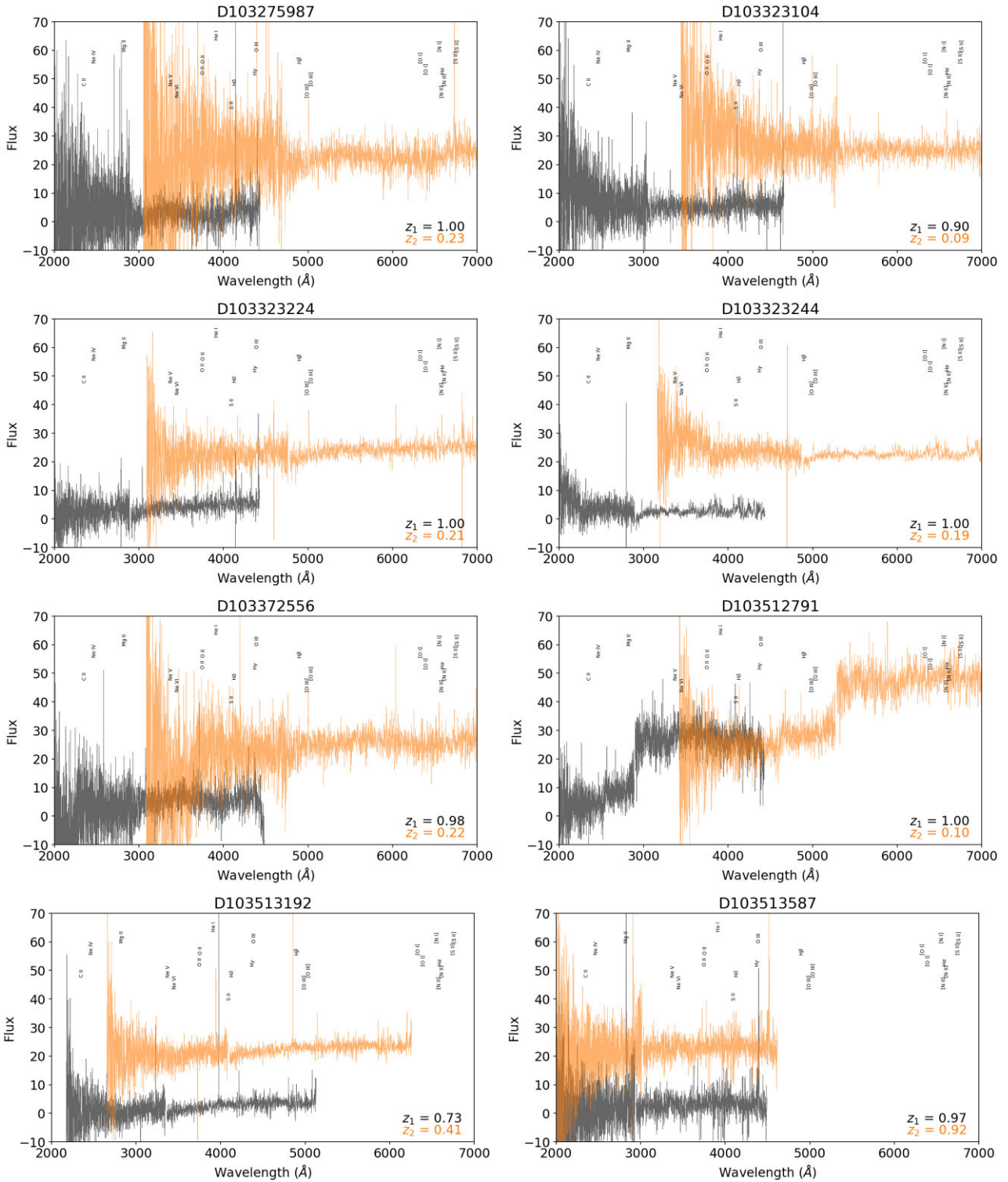**Figure A1** *– continued*
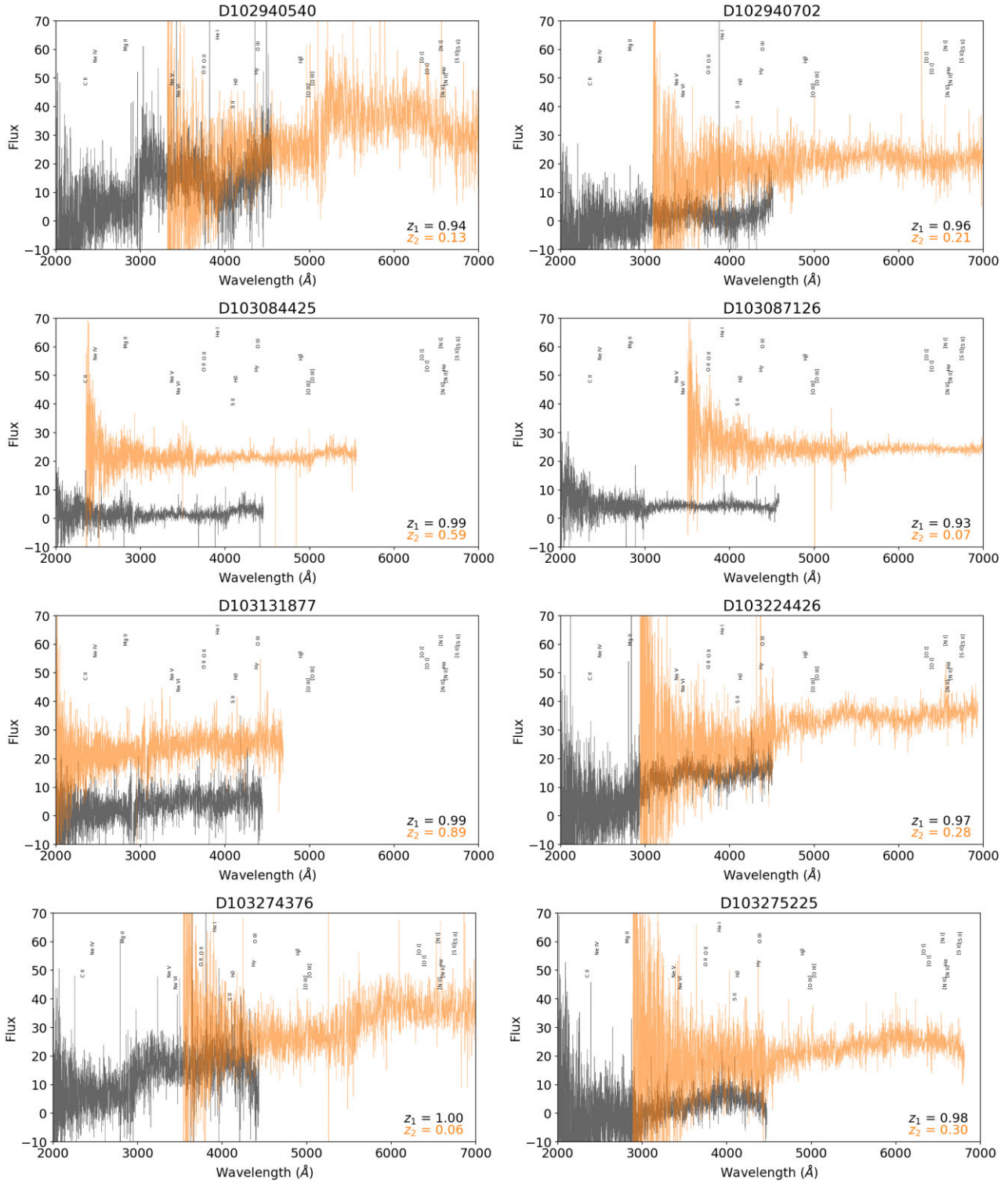
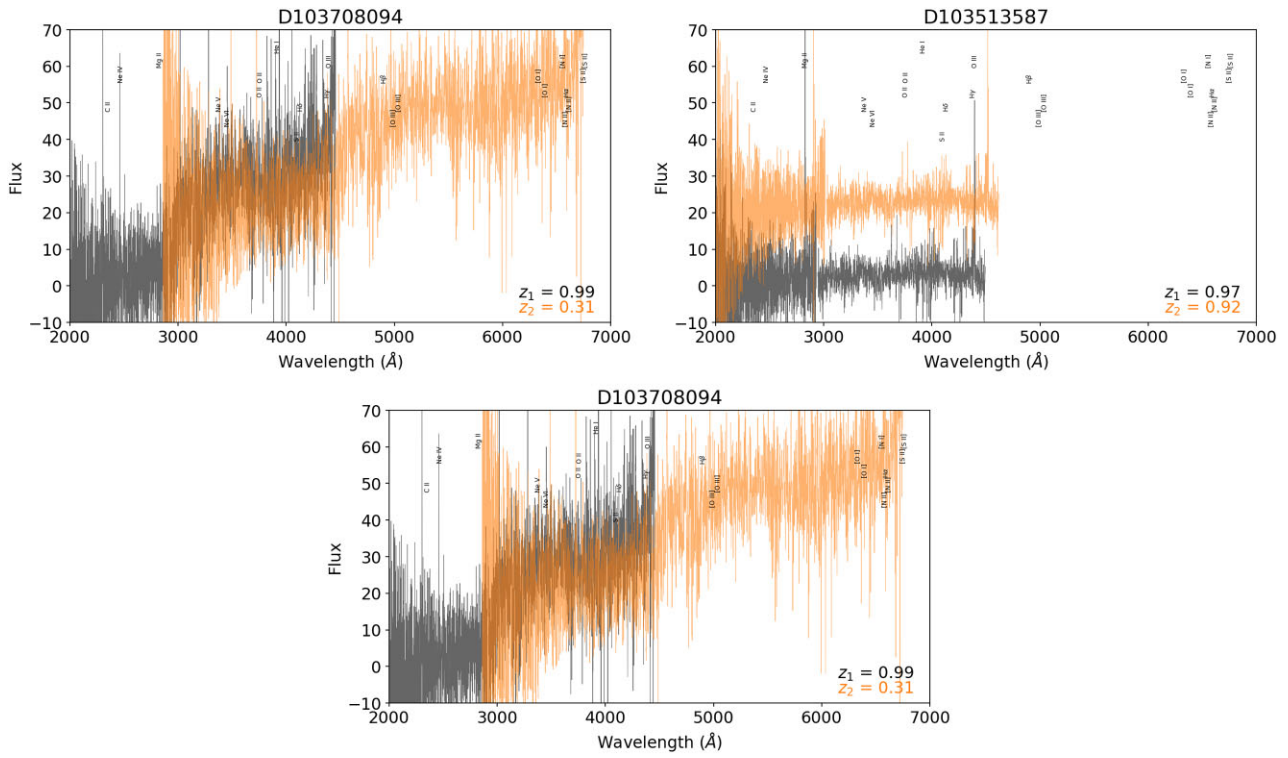**Figure A1** – *continued*

Figure A1 *– continued*

Figure A1 *– continued*

This paper has been typeset from a TEX/LATEX file prepared by the author.